THESIS

COFILIN-ACTIN RODS: QUANTIFICATION AND COMPARISON TO TAU PATHOLOGY IN A HUMAN LONGITUDINAL AGING STUDY AND DEVELOPING PROBES TO MEASURE LOCALIZATION AND ACTIVITY OF NADPH OXIDASE 2, A COMPONENT OF THE PRION-DEPENDENT ROD INDUCING PATHWAY

Submitted by

Adlei B. Carlson

Department of Biochemistry and Molecular Biology

In partial fulfillment of the requirements

For the Degree of Master of Science

Colorado State University

Fort Collins, Colorado

Fall 2015

Master's Committee:

Advisor: James R. Bamburg

Santiago Di Pietro
Gregory C. Amberg

ABSTRACT

COFILIN-ACTIN RODS: QUANTIFICATION AND COMPARISON TO TAU PATHOLOGY IN A HUMAN LONGITUDINAL AGING STUDY AND DEVELOPING PROBES TO MEASURE LOCALIZATION AND ACTIVITY OF NADPH OXIDASE 2, A COMPONENT OF THE PRION-DEPENDENT ROD INDUCING PATHWAY

The presence of extracellular amyloid plaques composed mainly of fibrils of the β-amyloid peptide (Aβ) as well as intracellular neurofibrillary tangles composed mainly of hyperphosphorylated tau protein, are used for post-mortem confirmation of the diagnosis of Alzheimer's disease (AD). However, a shift in disease hypothesis has changed over the years. It is now generally accepted that soluble forms of Aβ oligomers and not fibrils, which are deposited in plaques, are most responsible for the synaptic loss and eventual neuronal death that accompanies AD progression. In cultured mammalian neurons, treatment with this more relevant, soluble form of Aβ induces the formation of cofilin-actin rods within neurons. Rods may grow to occlude the neurite and block transport, leading to loss of microtubules and synapses. Tau is a microtubule binding protein whose hyperphosphorylation depends upon its release from microtubules. Thus, rod formation might play a role in the loss of synapses and the development of tau pathology in AD. To determine if cofilin-actin rods might play a role in AD progression, we obtained samples of frontal cortex and the hippocampal formation from nearly identical regions of multiple subjects who were part of a longitudinal study and thus could be grouped as non-cognitively impaired (NCI), early AD (eAD), or mid to late AD. All samples were obtained with a short postmortem interval and the average age of subjects in each group was between 86 and 91 years. We prepared 30 μm sections of cortical and hippocampal tissue, and following immunofluorescence staining for cofilin and phosphorylated tau protein, quantified rod and neuropil thread areas in brain sections from each subject. Rods in the hippocampal formation were most prevalent in the

entorhinal cortex, the first brain region to show pathology during development of AD. Comparison of rod and neuropil thread pathology in the frontal cortex revealed a correlation of neuropil thread pathology with disease transition. However, there was no correlation between rod density and disease transition, while the cortical sections revealed a surprisingly high deposition of cofilin rod pathology across all subject cohorts. This may suggest that rods play a different role within brain cortical regions than what was observed in the hippocampus.

Additionally, recent work has revealed the implication of a prion-dependent rod inducing pathway dependent on the activation of the reactive oxygen producing NADPH oxidase 2 (NOX). If prion-protein density is responsible for whether a rod forms, can we investigate the NOX intensity and duration of activity in relation to where rods form in a neurite? For future study we sought to develop the sensitive NOX probes, p47-roGFP and NOX-2-redtrack. These probes will give us new tools to analyze the effects that NOX activity and expression have on rod formation. The adenoviral constructs for expression of these two probes have been made and characterized within mammalian cell lines. Evidence presented here provides the basis for the use of these probes to analyze NOX activity as it relates to the generation of rods within neurites.

ACKNOWLEDGEMENTS

I am very grateful for a number of people who have helped along in my journey to complete this thesis. First and foremost, I am grateful to my wife. It takes a special person to put up with various weekends and late evenings in the lab, she has been exceptionally understanding and encouraging throughout this process. Secondly, I am very grateful to both Dr. James Bamburg and his wife Laurie Minamide. I was a fresh graduate with no lab experience when Dr. Bamburg took a chance on a kid who was interested in Alzheimer's. The lab has provided me a great opportunity to learn and face challenges for which I could have never prepared. The great mentorship provided by the both of them has added so much to my work here at CSU and what it will become in the future. I am eternally grateful for the compassion, training, leadership and coaching; thank you for giving me the independence to make mistakes, but always being prepared to follow it up with teaching. Lastly, I am very grateful for the other lab members Alisa Shaw, O'Neil Wiggan, Keifer Walsh, Lindsey Whittington and Jessica Zanon, each of whom played a role in my learning and training throughout this journey.

TABLE OF CONTENTS

Abstract ii
Acknowledgements iv
Table of Contents v
List of Figures vi
List of Abbreviations vii
Chapter 1: Introduction 1
Cholinergic Innervation Disruption Hypothesis 1
Amyloid Cascade Hypothesis 3
Soluble Aβ Hypothesis 6
Role of Oxidative Stress in Neurodegenerative Disorders 9
Cofilin-Actin Rod Hypothesis 11
Thesis Focus 13
Chapter 2: Materials and Methods 15
Human Tissue Samples 15
Immunostaining 16
Adenovirus Generation 18
Chapter 3: Rod Analysis in Human Brain Frontal Cortex 21
Introduction to Receipt and Processing of Samples 22
Hippocampal Tissue Analysis (Development of Analysis Strategy) 22
Analysis in the Frontal Cortex (Reevaluation of Imaging Strategy) 29
Addendum 1 41
Chapter 4: Adenoviral NADPH Oxidase Probes 43
NADPH Oxidase Introduction 43
Construct Generation 43
Construct Characterization 44
Chapter 5: Discussion and Future Directions 50
References 55

LIST OF FIGURES

Figure 1.1	Differential APP Processing Generates Non-Amyloidogenic or Amyloidogenic Aβ Fragments	4
Figure 3.1	Cofilin-Actin Rod and Tau Pathology in the Human Brain	23
Figure 3.2	Specificity of Antibody Staining and Rod Composition	25
Figure 3.3	Regions of Interest in the Hippocampus	26
Figure 3.4	Rod and Tau Pathology Quantification within the Hippocampus	28
Figure 3.5	Initial Frontal Cortex Imaging Strategy	29
Figure 3.6	Lamina of the Frontal Cortex	31
Figure 3.7	Imaging the Frontal Cortex following Cresyl Violet Staining	32
Figure 3.8	Imaging Frontal Cortex Sample with Olympus VS120 Scanning Microscope	34
Figure 3.9	Cresyl Violet re-stain of Previously Immunostained Samples	35
Figure 3.10	Rod Density within the Frontal Cortex NCI, eAD and AD Subjects	37
Figure 3.11	Frontal Cortex Rod Quantification in Outer and Inner Cortical Regions	38
Figure 3.12	Neurofibrillary and Neuropil Tau Pathology Quantification within the Frontal Cortex	39
Figure 3.13	Neuropil Thread and Tangle Pathology Quantification in External and Internal Cortical Regions	40
Figure 4.1	Western Blot Analysis	45
Figure 4.2	Redtrack RFP Expression in HeLa Cells	46
Figure 4.3	ROS Sensing Activity of p47-roGFP	48
Figure 4.4	p47-roGFP Infected Cells Exhibit Membrane Translocation When Activated	49

LIST OF ABBREVIATIONS

Aβ	Beta-amyloid
Aβd/t	Beta-amyloid dimer/trimer
AD	Alzheimer Disease
ADF	Actin Depolymerizing Factor
APP	Amyloid Precursor Protein
eAD	Early Alzheimer's Disease
ERC	Entorhinal Cortex
FAD	Familial Alzheimer's Disease
LTP	Long-Term Potentiation
MMSE	Mini-Mental Status Exam
MOI	Multiplicity of Infection
NCI	Non-cognitively impaired
NFT	Neurofibrillary Tangle
NF-κB	Nuclear Factor-κB
NMDA	N-methly-D-aspartate
NOX	NADPH oxidase
NT	Neuropil Thread
PrP^C	Cellular Prion Protein
Pyr	Pyramidal
ROS	Reactive Oxygen Species
SSH	Slingshot
SUB	Subiculum
TBI	Traumatic Brain Injury (mTBI, mild)
TNFα	Tumor Necrosis Factor-alpha
TNFRI	Tumor Necrosis Factor Receptor I
TNFRII	Tumor Necrosis Factor Receptor II
UKADC	University of Kentucky Alzheimer Disease Center

Chapter 1: Introduction

Alzheimer's Disease

Alzheimer's disease (AD) is the most common form of dementia, primarily affecting adults over the age of 65. It is a progressive and debilitating mental illness of cognitive degeneration manifesting itself in memory lapses, mood swings, and the inability to effectively communicate. AD is an excruciating illness for the diagnosed and their families. However, as the number of adults over the age of 65 is expected to increase with the aging baby boomer population, AD will also stress the health system economically. This year (2015) AD costs are expected to reach $226 billion (1). With the projection of AD cases continuing to double each year to 2050, the pressure on the healthcare system will only be intensified (2). In light of this bleak outlook, the need for advancement in AD research cannot be understated.

Cholinergic Innervation Disruption Hypothesis

AD is marked by the eventual death of neuronal cells leading to significant reductions in brain cortical thickness and volume (3). The level of deterioration taking place in AD is striking, and has provided a basis for those attempting to understand the disease through its course of destructive brain atrophy. In an attempt to explain the neuronal degeneration taking place in AD, various hypothesis have been proposed over the years. The memory and cognition deficits associated with the disease point to a disruption of neuronal cell communication or synaptic transmission. Early on, many observations noted a higher degree of neuronal cell loss in AD individuals within the cerebral cortex, primarily the frontal and temporal cortices (4). Supporting evidence showed the specific degeneration of cholinergic neurons in the cortex, neurons that primarily release the neurotransmitter acetylcholine at their synapses (5). This finding led to the Cholinergic Innervation Disruption Hypothesis, one of the first attempts to explain the age-

related and sporadic neurodegeneration of Alzheimer's disease. The relevance of this hypothesis hinged on three key observations; (a) specific dysfunction in cholinergic markers in patients suffering from memory loss; (b) disrupting cholinergic function in young people artificially created similar symptoms found in the elderly with cognitive impairment; and (c) those suffering from cognitive impairment could be rescued with cholinergic function enhancement (6). Various observations of these points led to the idea that the disease was targeting specific acetylcholine-releasing neurons (4). This led to the development of therapies (acetylcholinesterase inhibitors such as donepezil, known as Aricept®) targeting the cholinergic neurons, attempting to alleviate what was viewed as acetylcholine disrupted synaptic transmission.

However, the development of cholinergic targeted treatments has provided some strong evidence that cholinergic disruption is likely not the causative disease agent, as the therapies only briefly slow disease progression, and fail to stop continued degeneration and neuronal cell loss (7). Furthermore, while the loss of cholinergic markers is documented in AD, it does not appear to be significant in early disease pathology, indicating it may simply be an effect of the local toxic environment (8). In addition, new evidence has indicated disease pathology begins in the entorhinal cortex and hippocampal brain regions; before progressing to large neocortical areas such as the temporal and frontal cortices (9-11, 12). From the beginning of AD research through the development of the cholinergic innervation hypothesis, other pathological changes were noted in AD brain that included the presence of neuritic amyloid plaques and neurofibrillary tangles (4). However, the presence of plaques was reconciled as the result of cholinergic marker deposition and decreased activity acting as upstream contributors to the propagation of plaque and tangle pathology (4). With evidence emerging contrary to the cholinergic innervation hypothesis, amyloid plaques again returned as central to the ideas surrounding AD development.

It has been over a hundred years since Alois Alzheimer first observed fibrillar pathology in the brain of a female patient in what would become described as amyloid plaques (13). However, while the presence of amyloid plaques seems synonymous with AD, their origin and role in disease development have been controversial. The presence of plaques and neurofibrillary tangles, are still used to confirm the AD diagnosis in post-mortem patients. A probable AD diagnosis can be made early-on in patients with progressive cognitive, language and executive function decline (14). When used in conjunction with modern techniques such as positron emission tomography, functional MRI and disease markers in cerebrospinal fluid, early disease diagnosis is improving in accuracy and efficiency (3). Due to its near universal association with AD, many have considered the importance of plaque pathology goes beyond diagnosis and is central to disease origination, development and progression.

Amyloid Cascade Hypothesis

Following the cholinergic innervation hypothesis, it was proposed that the primary causative agent in AD was the presence of amyloid plaques in what became known as the Amyloid Cascade Hypothesis. This hypothesis proposes that Amyloid-beta (Aβ) deposition into insoluble amyloid plaques directly causes the development of neurofibrillary tangles, neuronal cell death, and dementia (15).

The amyloid precursor protein (APP) is commonly recognized as the early role player in AD, as it generates the basic protein fragment amyloid-beta (Aβ) in the easily stained extracellular deposits known as plaques. APP is a single transmembrane protein which can undergo processing by opposing pathways (**Figure 1.1**) to generate either pathogenic or non-pathogenic APP protein fragments (16).

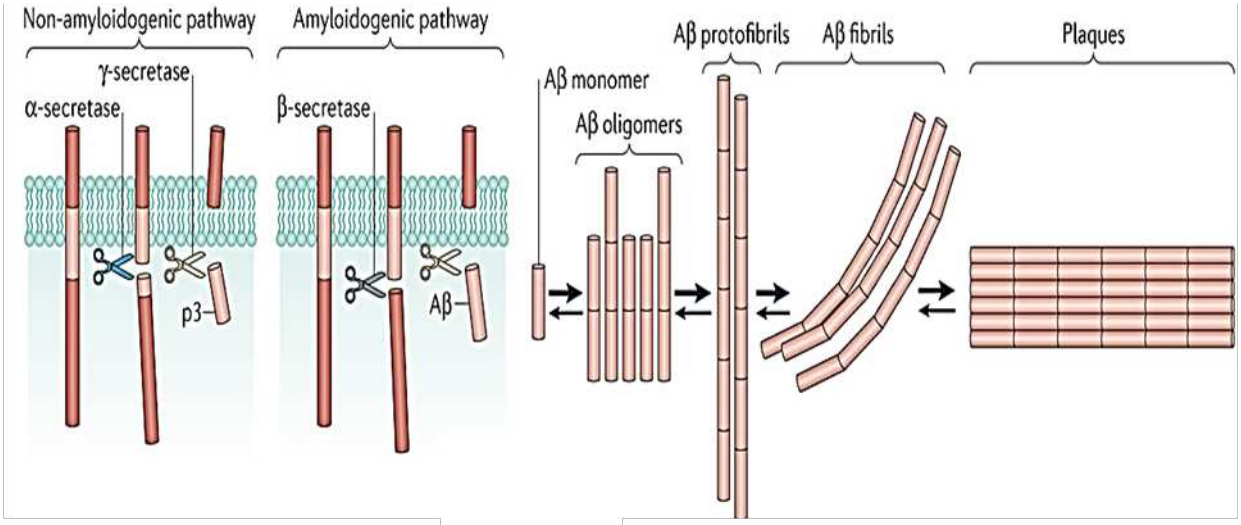

Figure 1.1: Differential APP Processing Generates Non-Amyloidogenic or Amyloidogenic Aβ Fragments. When APP processing initiates with α-secretase cleavage, the generated fragment is easily degraded within the cell. This generates what is considered non-amyloidogenic Aβ fragments. However, when APP undergoes initial β-secretase cleavage, Aβ fragments between 39-43 amino acids are generated. These fragments are considered amyloidogenic due to their propensity to oligomerize and aggregate into plaques. Adapted from *Figure 1a Heppner et al 2015* (17).

When APP is cut by the proteases α-secretase and γ-secretase, the fragments that are generated are soluble, non-pathogenic and get degraded and are cleared from the tissue. However, when the proteases β-secretase (or cathepsin B (18)) and γ-secretase cleave APP, one of the products is a pathogenic beta-amyloid (Aβ) peptide (19). Depending on the exact residue within the membrane spanning domain that is cleaved by γ-secretase, the Aβ peptides range from 39-43 amino acids with the 40 and 42 length peptides as the major species. Pathogenic Aβ is amyloidogenic and can undergo oligomerization in the extracellular space generating the hallmark insoluble Amyloid Plaques. Aβ fragments of 42 amino acids, while less common than the 1-40 species, exhibit increased oligomerization and are considered the more neurotoxic of Aβ species (20).

In addition to the amyloid plaques, AD postmortem confirmation also requires the presence of intracellular Neurofibrillary Tangles (NFTs) composed of the protein tau. Neurons rely on an extensive transport network to supply synapses, the points of communication between neurons necessary for their function. These transport networks in axons and dendrites are made up primarily of microtubules. Tau functions as a microtubule stabilizing protein, releasing from microtubules when phosphorylated in its microtubule binding domain and able to bind microtubules when dephosphorylated (21, 22). Microtubule stabilization by tau helps maintain their ability to carry on axonal transport of vesicles over long distances and to modulate their assembly dynamics (21).

However, tau has amyloidogenic regions and, within the context of AD, tau elicits internal neuronal toxicity as tau aggregates in Neurofibrillary Tangles (NFTs) and Neuropil Threads (NTs). Tau aggregation likely begins with an increase in unbound and multi-phosphorylated tau, leading to initial deposits of NTs which can progress further into NFTs (21). However, hyperphosphorylated tau can also be released externally and has neurotoxic effects (23, 24).

The strongest evidence in support of the amyloid cascade hypothesis comes from the rare heritable forms of AD. Generally AD is classified as either familial (genetic based) early-onset AD (FAD) or sporadic (late onset) AD (SAD). In FAD the heritability is linked to genetic mutations in APP, in the catalytic γ-secretase isoforms presenilin 1 and 2 (3), both of which lead to excess Aβ formation, or in the presence of a specific allele (ε4) of a brain produced apolipoprotein E, which may act by increasing the oligomerization and toxicity of Aβ fragments (25) or by decreasing their clearance (26). Furthermore, trisomy 21 (Down syndrome) is also associated with early-onset AD due to APP gene duplication, as it is located on chromosome 21 (3). Each of these heritable factors not only lowers the age of disease onset, but also increases

the level of toxic Aβ fragments. This evidence serves as the basis for the Alzheimer's disease amyloid cascade hypothesis.

Exactly how the amyloid plaques were supposed to act as the causative agent in AD was never fully explained. The FAD associated mutations and trisomy 21 contribute to greater production and deposition of Aβ while also lowering the age of disease onset, indicating the crucial role of amyloid in disease development (15, 27). It is thought the presence of plaques may activate neuronal immune cells initiating an inflammatory response and/or physically blocking neuronal synaptic connections (28). Yet, support for the amyloid cascade hypothesis has been waning since many studies have shown that plaque development does not correlate either with dementia or with neuronal death (29). Plaques sometimes in very high numbers can be present before any sign of cognitive decline (19). John Hardy a co-author of the original amyloid cascade hypothesis reconsidered the role of plaques in toxicity, acknowledging that it is likely the soluble Aβ oligomers act as the toxic disease agent (30). This has transitioned into a variation of the amyloid cascade hypothesis of AD, recognizing toxic soluble Aβ fragments as central to disease progression.

Soluble Aβ Hypothesis

A major shift in the AD hypothesis was supported by evidence that an early event in AD development was dysfunction at neuronal synaptic connections (31). This shift was further supported by evidence that soluble Aβ oligomers, not plaques, may be acting at the synapse as observed in animal models and predicted for human AD (27).

Exactly how the synaptic disruption occurs is not fully understood. It has been demonstrated that oligomeric Aβ disrupts long term potentiation (LTP) the major pathway activated in learning and new memory formation which reflect cognitive ability (32, 33).

Soluble Aβ may primarily elicit toxicity by stimulating the toxic aggregation of tau, and its effects on cognitive ability is likely dependent on tau (34). In AD mice expressing toxic Aβ, the suppression of tau expression was able to rescue lifespan, memory, and seizure deficits (34). Tau aggregation alone is known to have toxic effects on the brain. In the disease frontotemporal dementia, a genetic tau mutation contributes to abnormal tau protein aggregation, causing neurodegeneration without Aβ pathology (35). This tauopathy lends support to the idea that tau aggregation alone is sufficient to cause synapse loss and neurodegeneration. Yet, the mechanism in AD by which Aβ might induce tau aggregation is still not resolved. Aβ may mediate tau toxicity through tau mislocalization, early accumulation, hyperphosphorylation, or neuronal inflammation (34, 36, 37). While each of these events could play a single or combinatorial role in mediating Aβ toxicity, there is an additional but less understood pathology which may connect Aβ to synaptic loss and alterations in tau aggregation, that of cofilin-actin rods. Cofilin-actin rods may play a role in synapse loss and neuronal toxicity due to their ability to disrupt microtubules, occlude neurites, block neuronal transport, and impair synaptic transmission through sequestering of cofilin (38, 39).

Actin depolymerizing factor (ADF) and cofilin are members of the same (ADF/cofilin) family of actin-binding proteins, influencing both the polymerization and disassembly of actin networks (39). Because cofilin is the major isoform found in neurons, present at about 5 to 12 fold greater amounts than ADF (40, 41), we will subsequently refer only to cofilin. Actin is a cytoskeletal protein with roles in cell motility, morphology and transport (42). Within neurons, cofilin-mediated actin dynamics controls most aspects of development including neuritogenesis, axonogenesis, growth cone pathfinding to find synaptic targets, and the development of dendritic spines. The structural reorganization of dendritic spines during long-term potentiation (LTP) and long-term depression (LTD) (43-46) is essential to the network remodeling implicated in memory formation (47). The ability of actin networks within spines to reorganize efficiently

depends partly on the severing and nucleation events mediated by cofilin. Cofilin is regulated via the phosphorylation state of serine 3 (S3 in the encoded protein), largely dependent for inactivation on the activity of LIM kinase and activation by the phosphatase slingshot (39). Because of the ability of cofilin at high concentrations to bind to F-actin cooperatively and to stabilize small pieces of cofilin-saturated F-actin, it better serves as a persistent severing protein at low concentrations relative to F-actin (39, 48).

In neurons, cofilin concentrations are about 20% of that of actin. When cofilin is locally activated it can bind and sever actin filaments but preserve shorter pieces of actin that become saturated with cofilin. Alternatively, if cofilin is activated in a region containing high actin monomer, it can bind to monomer forming a cofilin-actin complex that has its unique critical concentration for assembly into cofilin-actin (1:1) filaments (49). These filaments can form bundles (rods) in regions containing levels of reactive oxygen species (ROS) above some threshold; much of the cofilin within rods isolated from neurons occurs as disulfide linked dimers showing that its oxidative cross-linking occurs within rods in vivo (50). Within neurons rods may form in response to oxidative stress (peroxide or NO), excitotoxic levels of glutamate, or ATP-depletion stresses (51), but also in response to Aβ, proinflammatory cytokines and overexpressed prion protein (52-54). However, rod formation may be a protective effect gone awry in cells. Within energetically stressed cells, rods may form to reduce ATP utilization that occurs during actin turnover (55). Yet, in neurites with limited clearance, rod formation may prove to be too disruptive. Overexpression of cofilin induces rod formation in cultured rat and *Aplysia* neurons which elicits synaptic structural and function deficits (38, 56). Within rat neurons synaptic disruption occurred specifically within the neurites where rods formed (56). This evidence indicates rod formation within neurites may contribute to distal synaptic disruption, alluding to a possible role for rods in the synaptic disruption observed in AD. Furthermore, rod-shaped cofilin stained structures have been observed in the hippocampus of

brains of AD subjects but not in controls, suggesting rods might be important in cognitive decline (51).

In addition to rods being observed in brain tissue from AD individuals, rod pathology has also been extended to animal models. Within drosophila and mouse tauopathy models, which correlate well with the neurotoxic changes observed in AD, rod density has been associated with tau mediated neuronal toxicity (57), with rods also being separately observed in an AD mouse model (53). Additionally, rods have been induced by soluble Aβ oligomers in cultured rat and mouse hippocampal neurons (52, 58). Recently, work by Walsh et al has demonstrated two independent pathways for ROS production during rod formation in neurons, one that is dependent upon expression of the cellular prion protein (PrP^C) and one that it is independent of PrP^C (54).

Role of oxidative stress in neurodegenerative disorders

Due to its high energy need, the brain utilizes a very high percentage of the oxygen we inhale each day, about 20% of the total for an organ that is only 2% of the body mass. Thus it is not surprising that ROS levels within the brain are also higher than other tissues. However, the age-related decline in REDOX regulatory factors (e.g. SOD, catalase, glutathione, etc.) that protect the brain from the excess ROS contribute to the age-related onset of many neurodegenerative diseases such as AD and Parkinson's disease, both of which exhibit neuronal ROS related damage (59). In addition to oxidative stress being associated with cognitive impairment (60), it has also been observed that levels of oxidative stress markers increase with AD progression suggesting oxidative stress may play a role in continuous disease progression (61).

Due to the depressed antioxidant activity in AD patients (59), oxidative stress may play a persistent role in the disease in a feed-forward activity by enhancing the toxicity of AD

pathology. Oxidative damage has been shown to play a role in the propagation of protein aggregation of both tau and Aβ (62). There is strong evidence indicating Aβ plays an initial role in not only eliciting oxidative stress, but also resulting in the release of superoxide ROS species from microglia (62). Activation of microglia is considered an early disease response as Aβ stimulates the release of inflammatory cytokines in addition to production of excess ROS (62). It has also been suggested that Aβ alone may act as an oxidizing agent contributing to the generation of free radicals (63). The induction of microglial activity by Aβ has been shown to specifically activate the ROS producing enzyme NADPH oxidase (NOX) and the release of the cytokine tumor necrosis factor-α (TNF-α) (64, 65). Within the context of AD, NOX activity up regulation has been associated with early disease initiation and progression (66).

The inflammatory cytokine TNF-α mediates immune responses throughout the body. Within the brain TNF-α release recruits and activates immune cells localizing inflammation and can have separate cellular effects dependent upon the activation of the TNF receptors I or II (65). TNFRI activation stimulates an apoptotic cellular pathway through nuclear factor-κB (NF-κB), while TNFRII exhibits cell survival and protective activity (65). However, glial TNF-α release in the neuronal disease state robustly activates TNFRI over TNFRII (65).

Oxidative stress also plays a significant role in additional neuropathology of traumatic brain injury (TBI). TBI results from force trauma which elicits downstream cascade events of inflammation, oxidative stress, excitotoxicity and ionic balance disruption, contributing to eventual neuronal cell death (67). Following the severity of TBI, neuronal degeneration and cognitive impairment become progressively worse as the pathology spreads. Within a TBI mouse model it has been suggested that within the hippocampus NOX activity is elevated following trauma (68). The degeneration which occurs in TBI through neuronal cell loss with NOX activation may very well parallel NOX initiation within AD. Activation of the NOX pathway

induces rods within neurons (54), and may provide a common link between TBI and AD degeneration in a converging neuronal degenerative pathway.

Cofilin-actin rod hypothesis

Several changes occurring in AD brain have been identified that when replicated in model systems cause cofilin-actin rod pathology and thus provide support for the hypothesis that rods might be the cause of synaptic dysfunction, either through inhibiting transport or through sequestering of cofilin and inhibiting its function in spines.

In addition to ROS production, formation of cofilin-actin rods requires the activation (dephosphorylation) of cofilin. The dephospho-form is the only cofilin species found in rods (53) and rod formation is inhibited by overexpressing an active form of LIMK (52).
LIMK activity declines during AD progression brought about by a decline in its upstream regulatory kinase PAK1. If PAK1 is downregulated in a model system, cofilin-actin rods and aggregates (cofilin pathology) occur (69). Chronophin, a cofilin phosphatase different from slingshot, is regulated by binding to HSP90 in neurons. Release from HSP90 triggers rod formation, again showing that hyperactivation of cofilin can be rod-inducing (70). Indeed, oxidative stress (peroxide) which increases in AD brain can directly regulate the activity of the cofilin phosphatase slingshot; when activated in neurons slingshot causes cofilin-actin rod formation in neurites (71). MicroRNAs also regulate gene expression and two of these have been identified that downregulate cofilin expression in neurons. When these microRNAs, both of which decline in brains of AD subjects, are inhibited in neurons, cofilin overexpression ensues and this also drives rod formation (72).

As mentioned previously, there is an increase in oxidative stress markers and an increase in NADPH oxidase (NOX) during the development of mild cognitive impairment and AD. In

addition to its ability to directly impact cofilin dephosphorylation and its oxidation to form disulfide bonds in rods, ROS can have other effects that also enhance rod signaling. Whereas synthetic $A\beta_{1-42}$ has been shown to induce rods when used at 500 nM to 1 μM concentration, a more natural form of Aβ that is isolated from the medium of cells that express human APP carrying the FAD Swedish mutation (33) has a greater than 1000 fold increase in rod-inducing activity (52). The major Aβ species in this material are the SDS-stable dimers and trimers. Oxidation of synthetic human $A\beta_{1-42}$ to generate dimer and trimer increased its rod-inducing activity by 600 fold (52) suggesting that increased oxidative stress may promote both rod-inducing signaling as well as cofilin oxidation and rod formation.

Although mitochondrial inhibitors, hypoxia/anoxia and excitotoxic levels of glutamate induce rods, the pathway utilized for ROS production (probably mitochondrial) is different than the pathway used by Aβ, TNFα and other proinflammatory cytokines. This later pathway depends upon both the presence of the cellular prion protein (PrP^{C}) and the activity of NOX (54). NOX is a ROS producing enzyme which plays an important role in the ability of immune cells such as macrophages and neutrophils to eliminate invading microorganisms (73). NOX exists in 7 isoforms, but the NOX1, NOX2 and NOX4 isoforms are specifically found in neurons (13, 74). Although the NOX isoform involved in rod formation was not specifically identified, the ability of a dominant negative $p22^{PHOX}$ subunit to block rod formation when neurons were treated with Aβ or TNFα suggested that it would be NOX1-3, the isoforms requiring $p22^{PHOX}$ (54). Furthermore, a NOX inhibitor specific for NOX 1-2 also blocks rod formation in neurons, further narrowing the selection down to these two isoforms.

The NOX enzyme is a multisubunit protein which depends on the association of multiple cytosolic components for activity. The major NOX subunit, also known as $gp91^{phox}$, constitutively associates in the membrane with the $p22^{phox}$ subunit, creating the flavocytochrome b558 subunit

(73). The additional regulatory subunits p40, p47, and p67 exist in the cytosol, translocating to the membrane along with a Rac GTPase in the GTP form and the membrane associated Rap1A, when NOX is activated to produce ROS (73, 75). The p47 subunit is considered the "organizing" subunit of the NOX cytosolic component and when phosphorylated stimulates the translocation of the p67 and p40 subunits to the membrane (73). p67 activity is largely dependent on the GTPase activity of Rac. In its GTP bound state, active Rac binds p67 likely inducing a conformational change enabling p67 binding and activation of NOX (76). How TNF-α activates NOX is not completely understood, but is believed to occur through phosphorylation of p47 by protein kinase C-ζ, a tyrosine kinase, and p38-mitogen activated protein kinase (77).

Focus of this thesis

If rods do indeed play a significant role in the progression of AD, we would expect to find different levels of rod deposition in human AD brain similar to other pathologies such as tau and Aβ. Rod-induced synaptic toxicity may play a critical role in mediating the extracellular Aβ toxicity to intracellular tau toxicity. With human brain tissue samples from the hippocampus and frontal cortex we sought to make a correlation with disease transition and rod deposition. The samples received had short post-mortem intervals to fixation and were obtained from three different subject cohorts; non-cognitively impaired (NCI), early AD (eAD) and late-stage AD. All subjects were enrolled in a longitudinal aging study and were annually evaluated using the Mini Mental State Exam (MMSE). This unique data set offers the chance to analyze rod deposition in human brain to see if it correlates to disease progression. With this analysis we hope to determine if rods correlate with the disease transitional phase from non-cognitively impaired to early AD.

Secondly, the recent work in our lab has indicated NOX activity as a rod inducer capable of responding to various extracellular and inflammatory stimuli (Aβ, TNFα). To expand upon the initial observations of NOX 2 activity, we sought to develop a specialized NOX probes to observe and analyze NOX within the neurite. We developed a sensitive NOX subunit probe to observe NOX activation and changes to ROS generation in vivo. Additionally, we developed a NOX overexpression probe for future studies to analyze the effect of NOX overexpression on rod induction.

Chapter 2: Materials & Methods

Materials

Unless otherwise stated all chemicals are reagent grade and were obtained from Sigma-Aldrich Co., St. Louis, MO. Cell culture reagents were purchased from Life Technologies Invitrogen, Carlsbad, CA. The 1439 primary antibody is homemade (78). The 12E8 antibody was a gift from Elan Pharmaceuticals, Boston, MA. The Alexa secondary antibodies used were all purchased from Life Technologies, Carlsbad, CA. The NOX2 cybR plasmid and sequence primer were purchased from Origene, Rockville, MD. The p47-roGFP-pcDNA3.1 plasmid was generously received from the lab of George Rodney at Baylor College of Medicine.

Human Brain Samples

Fixed hippocampal and frontal cortex samples were obtained from the University of Kentucky Sanders-Brown Center on Aging. Postmortem intervals averaged 2.7 hrs and were no greater than 4 hrs. The subjects were enrolled in a longitudinal aging study and were assessed annually for mental status. Gross examination of the post-mortem brains was done by a neuropathologist and cases were excluded if they exhibited non-AD type pathologic conditions such as brain tumors, large strokes, etc. Individuals were classified as non-cognitively impaired (NCI), early AD (eAD), or AD based on antemortem cognitive testing and postmortem histopathology in accordance with parameters set by the National Institute of Neurological and Communicative Disorders and Stroke and the Alzheimer's Disease and Related Disorders Association (79). The Mini-Mental Status Examination (MMSE) score ranges for the NCI, eAD, and AD cohorts were 28-30, 22-24, and 2-19, respectively. Braak staging ranges were 0-V (NCI), II-VI (eAD), and V-VI (AD).

Immunostaining

Formaldehyde fixed brain tissue was cryoprotected at 4° C in 10% sucrose in phosphate buffered saline (PBS) 1-2 days and then in 20% sucrose in PBS overnight. The tissue pieces were subsequently frozen in O.C.T. Compound (Ted Pella, Inc) and 30 µm frozen sections prepared on a cryostat and adhered to Superfrost Plus slides (VWR). The sections were stored at -20° C until immunostaining. Sections were thawed for 15 min at room temperature (RT) and then rehydrated in PBS for 10 min. Sections to be immunostained for both cofilin (1439 antibody) and phosphorylated tau (S262,S356, 12E8 antibody) were permeabilized first with -20° C 80% methanol/20% PBS for 90 s followed by 0.05% Triton X-100 in PBS for 90 s with three PBS washes before and after the Triton X-100 treatment. After permeabilization, sections were blocked in 5% goat serum diluted in 1% BSA in Tris-buffered saline (TBS) (50 mM Tris, 50 mM NaCl, pH 7.5) for 1 hr at RT. Primary antibodies were then applied and incubated overnight at 4° C. Primary antibodies used were rabbit anti-ADF/Cofilin (1439, 2 ng/ml) and mouse anti-phosphorylated tau (12E8, 2 ng/ml). Secondary antibodies were Alexa 488 or Alexa 647-conjugated goat anti-rabbit or mouse IgG (Life Technologies) used at 1:500 with 2 ng/ml DAPI and incubated for 2 h at RT. To reduce autofluorescence, the sections were treated with 70% ethanol for 5 min and then 0.1% Sudan Black B in 70% ethanol for 12-15 min. The sections were rinsed briefly twice with 70% ethanol followed by TBS and 30 sec in water before applying 25 ml Prolong Antifade Gold (Life Technologies) and overlayed with an ethanol-cleaned coverslip.

Cresyl Violet Staining

To visualize frontal cortex laminar layers, Cresyl violet staining was utilized. Frontal cortex sections were rehydrated in PBS for 10 min, then dehydrated with 3-5 dips each in water, 70% ethanol, 95% ethanol, 100% ethanol and Hemo-D, then hydrated again in the opposite direction.

Sections were placed in Cresyl Violet (0.1% Cresyl Violet Acetate) stain for 10-15 min, and rinsed in water. Section were again dipped 3-5 times each in 70% ethanol, 95% ethanol, 100% ethanol, and Hemo-D. The sections were mounted on coverslips with 100 µL entellen and dried overnight. Additionally, this staining method was extended to previously immunostained frontal cortex samples mounted in ProLong Gold Antifade. Frontal cortex sample was placed in a 50 mL conical tube with water at 37 ^{o}C for two hours. After the two hour incubation, the tube was removed and left at room temperature overnight. The following morning the tube was returned to the water bath at 37 ^{o}C for a second two hour incubation. After the second incubation it was possible to remove the mounted cover slips with slight manipulation using a scalpel blade. Once the coverslips were removed, the sample was placed in TBS until staining. Cresyl Violet staining of the immunostained samples proceeded similar as above with successive dips in ethanol and Hemo-D. However, the amount of time the sample was placed in the stain was increased to 30 minutes. Following the stain the sample again underwent ethanol and Hemo-D dips, then mounted with 100 µL entellen and allowed to dry overnight.

Microscopy

For quantitative microscopy of the frontal cortex sections, the Olympus VS120 system was used to acquire data from 40X objective image stacks (20 µm) of larger areas (two 1.04 mm^2 areas per sample, 2.6 mm x 0.4 mm). Images were acquired with Olympus VS-Desktop software. Images were then exported as 16-bit tiffs, deconvolved, thresholded, and cofilin rods/inclusions and striated neuropil threads/neurofibrillary tangles quantified with Metamorph Software (Molecular Devices). Images of Cresyl Violet-stained sections were acquired on the Olympus VS120 system using bright field. Whole slide scans were performed with a 10X objective and cross-section scans were performed with 20X and 40X objectives. Images were exported as virtual slides (VS) and analyzed with OlyVIA software (Olympus).

Neuronal Cell Culture

Cultured rat hippocampal neurons were prepared from thawed frozen stocks of Sprague-Dawley E18 fetal brains. Cells were plated on poly-D-lysine coated coverslips at a density of 18,000-20,000 cells per coverslip in 35 mm drilled-out dishes (22 mm square coverslip attached to dish with aquarium sealant) or on 15 mm round coverslips in a 24-well culture dish. Coverslips were previously rinsed in 100% ethanol, water, 100% ethanol, and then flamed to dry. Neurons were cultured in neurobasal medium supplemented with B27 (Life Technologies), glutamine (125 µL/50 mL), penicillin/streptomycin (50 units/mL, 250 µL/50mL) and 10% fetal bovine serum (FBS; Hyclone Laboratories). Two hours after plating medium was removed and replaced with identical medium without FBS. Medium was replaced every three days. Cultures were maintained in 5% CO_2/95% air at 37° C.

HeLa Cell Culture

HeLa cells were cultured in HGDMEM 10% FBS medium and grown on 100 mm cell culture grade dishes. Cells were maintained in 5% CO_2/95% air at 37° C. For imaging cells were split with trypsin in PBS and plated on 35 mm glass bottom dishes (22 mm square coverslip attached to drilled out dish (15 mm diameter) with aquarium sealant).

Adenovirus Preparation

The p47-roGFP and NOX-2-redtrack expressing adenovirus was generated utilizing the AdEasy system. The p47-roGFP-pcDNA3.1 and NOX-2-pCMV6 plasmids underwent multiple rounds of specific endonuclease cutting, band purification and splicing, and bacterial transformations to generate expression constructs in pShuttle CMV plasmids for homologous recombination in BJ5183 E coli bacteria with the adenoviral backbone. The p47-roGFP-pcDNA3.1 plasmid was

received from our collaborator at the Baylor College of Medicine. Plasmid DNA was received on a piece of filter paper and rehydrated in 50 µL of water. The rehydrated plasmid was transformed into competent DH5α E coli cells. We received the NOX-2 (gp91phox, CYBB with terminal FLAG, c-myc tag) pCMV6 plasmid from Origene. The received 10 ug of plasmid was reconstituted in 100 ul water and stored at -20°C. Then the plasmid was transformed into DH5α competent cells. Each of the plasmids then underwent specific endonuclease cutting. The p47-roGFP construct was inserted into the pShuttle-CMV vector, while NOX-2 with the terminal tags was inserted into the RedTrack-CMV vector. The plasmids were then transformed into competent DH5α cells and amplified. Following amplification, the p47-roGFP-pShuttle-CMV and NOX-2-RedTrack-CMV plasmids were cut with PacI and electroporated into BJ5183 cells in which recombination with adenovirus core sequence (pAdEasy) occurred. Clones were selected and screened by restriction endonuclease digestion and those containing proper recombination were grown for plasmid DNA isolation, linearization and transfection into HEK293 cells utilizing lipofectamine. Screening for virus production was performed by fluorescence microscopy of the HEK cells and when significant areas of fluorescence protein expression was observed, cells were harvested, lysed by freeze-thaw and the released virus amplified through repeated HEK cell infection and harvesting. The viral titer was determined from the final lysate by serial dilution onto monolayers of HEK cells in 12 well culture dishes, fixation after 16 hrs and quantification of cell nuclei that stained for the viral replication factor E2a (80). Western blot analysis was performed using the fast-growing mouse neuroblastoma (N2a) cell line. Cells were grown to a density which covered the bottom of the well in a 6-well plate. Once desired density was reached cells were infected with MOI of 500 and 1000. Infected cells were monitored for fluorescence, and when majority of cells were fluorescent (greater than 50%), they were washed in PBS and lysed in an SDS-lysis buffer. Protein fragment was then extracted using chloroform/methanol extraction. SDS-PAGE gel was homemade (4% stacking and 10% separating) 10 µL of protein/buffer was loaded into each well. Gel was transferred to a

nitrocellulose membrane. A GFP antibody for p47-roGFP, FLAG and c-myc antibodies for the tagged NOX-2, and cofilin as a standard control were used for blotting.

Fluorescence Microscopy and Imaging of Cultured Neurons

Live cell imaging was performed on a Olympus IX81 inverted microscope equipped with a Yokagawa spinning disk head and a Cascade II EMCCD camera integrated by Intelligent Imaging Systems (3I) and operated by Slidebook software. To view RFP expression from NOX-2-RedTrack, Hela cells were infected with an MOI of 100. Cells were imaged using a 60X objective, with 561 nm excitation and bright-field (DIC) images. Cells were first focused under bright light, and then excited with the 561 nm laser. Cells which fluoresced red were deemed infected and positive for RFP expression. If the cell emitted no light it was determined to be uninfected, and therefore not expressing RFP.

Chapter 3: Rod Analysis in Human Brain Frontal Cortex

If rods do play a role in the development of AD, they likely would be found in post-mortem brain tissue alongside the classical AD hallmarks. Evidence of rod correlation with disease progression could provide necessary clues to bridge the gaps in Aβ and tau pathology. Recent work by Rahman et al suggests the tau pathology correlates with density of cofilin pathology in AD brain (81). While this is exciting preliminary data, the work done lacked samples from the critical early-AD stage important in analyzing disease progression and included both rods and cofilin aggregates in the total quantified cofilin pathology. Furthermore, the study surveyed many different brain regions without much detail from those regions most important in AD, the hippocampus and frontal cortex. Additionally, the study consisted of brain tissue with post-mortem harvesting time intervals averaging 22±12 hours for the controls and 27±16 hours for AD samples. Postmortem times over 6 hrs compromises the integrity of the tissue, which presents challenges in correlating the changes with disease progression, as well as the loss of significant pathology due to extended post-mortem intervals (82, 83). It is our goal to build upon these preliminary studies and quantify rod and tau pathology with AD progression in human short interval post-mortem tissue samples from the hippocampus and frontal cortex. We were fortunate to receive samples from three different cohorts of subjects: non-cognitively impaired (NCI), early-AD (eAD) and mid-advanced-stage AD. Furthermore, our samples were harvested with an average post-mortem interval of 2.7 hours with no samples exceeding 4 hours (Additional detailed patient information contained within Addendum 1). Samples from within the hippocampus and frontal cortex are significant for the roles these regions play in both memory and disease progression. The hippocampus has been widely studied because of its role in learning and memory. Additionally, it is also implicated in the initiation of AD pathology, specifically within the entorhinal cortex region of the hippocampal formation (84). As mentioned previously, cortical areas of the brain are often associated with late stage disease development.

However, frontal cortex activity has been implicated with emotional processing and response, executive control, and memory formation (85-87). Therefore, it can be assumed these brain regions may exhibit pathological changes in AD progression.

Receipt and Preparation of Human Brain Tissue

Human hippocampal and frontal cortex tissue samples were received from the University of Kentucky Sanders-Brown Center on Aging. Subjects are enrolled in a longitudinal aging study and agree to be annually assessed for mental status. NCI subjects are enrolled on volunteer basis within the University of Kentucky Alzheimer's Disease Center (UKADC) agreeing to annual mental status exams with additional semiannual physical and neurological exams within the UKADC volunteer aging program (88). Upon death subjects are processed at the UKADC Rapid Autopsy program, and samples are fixed in formaldehyde for 2 days, then transferred to PBS and shipped to us in casettes in PBS. Samples were refrigerated until they were embedded in OCT, frozen and cut into 30 μm sections with a cryostat. To prepare samples for immunostaining of cofilin and tau pathology, they were first thawed, permeabilized and then immunostained for cofilin and tau. Samples were obtained from 12 NCI, 5 eAD and 9 AD subjects. The average age for all cohorts was between 86 and 91, with the average age for NCI 86, eAD 91, and AD 87.

Hippocampal Tissue Analysis

Hippocampal tissue analysis is being completed by Laurie Minamide. Each sample was immunostained for cofilin and for phosphorylated tau using the 12E8 antibody (Elan Pharmaceuticals) directed against the peptide from a microtubule binding repeat domain (recognizes sequence containing phospho-serines 262 and 356 (89)). Two other phospho tau antibodies (pSer214 and pThr 217, both from Genescript) were used to verify similar staining

patterns. The slices were then examined by fluorescence microscopy for the presence of cofilin-actin rods (rods) and phosphorylated tau in the form of neuropil threads (NT) or neurofibrillary tangles (NFT). Images of the structures being examined are shown in **Figure 3.1**.

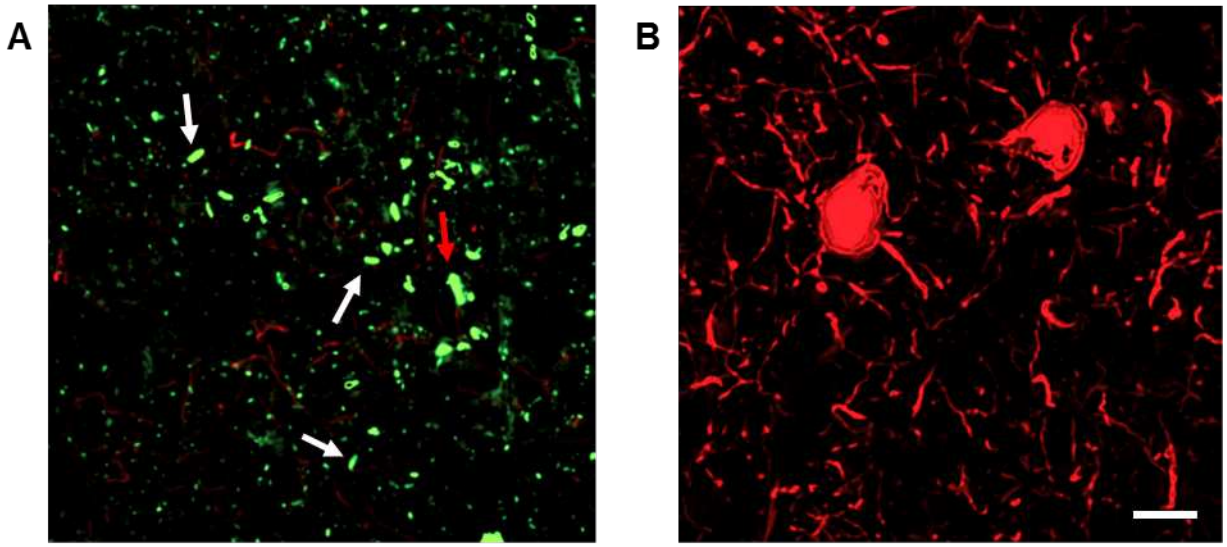

Figure 3.1 Cofilin-Actin Rod and Tau Pathology in the Human Frontal Cortex. (**A**) Shown in green are cofilin actin rods, rods were defined as having an area between 4-50 pixels or 2-24 µm. White arrows indicate rods quantified. The red arrow indicates a rod aggregate outside of the pixel boundary, and therefore not quantified. (**B**) Tau pathology is stained in red. The very large stained structures are neurofibrillary tangles and the neuropil threads are the smaller stained thread-like filaments. Bar = 15 µm.

For quantification purposes, background immunostaining was subtracted utilizing the Metamorph software. Initially we obtained high levels of background fluorescence that we found could be quenched by the application of 0.1% Sudan Black B in 70% ethanol for 10-15 min after immunostaining and then rinsing in 70% ethanol followed by TBS and water before applying Prolong Antifade Gold and a coverslip.

To distinguish between rods and cofilin aggregates, rods were defined as an area between 4-50 pixels an area covering 2-24 µm. A separate pathology of larger and amorphous cofilin-stained

aggregates, cofilin-actin inclusions, were quantified separately if they had pixel areas over 75. There were very few cofilin-positive stained structures that fell between these two categories. Three different antibodies were compared for cofilin immunostaining: a commercial rabbit antibody from Cytoskeleton, Inc (ACFL-02), a mouse monoclonal antibody (MAb22; 90), and a lab produced rabbit polyclonal antibody that was affinity purified (rabbit 1439; 78) (**Figure 3.2**).

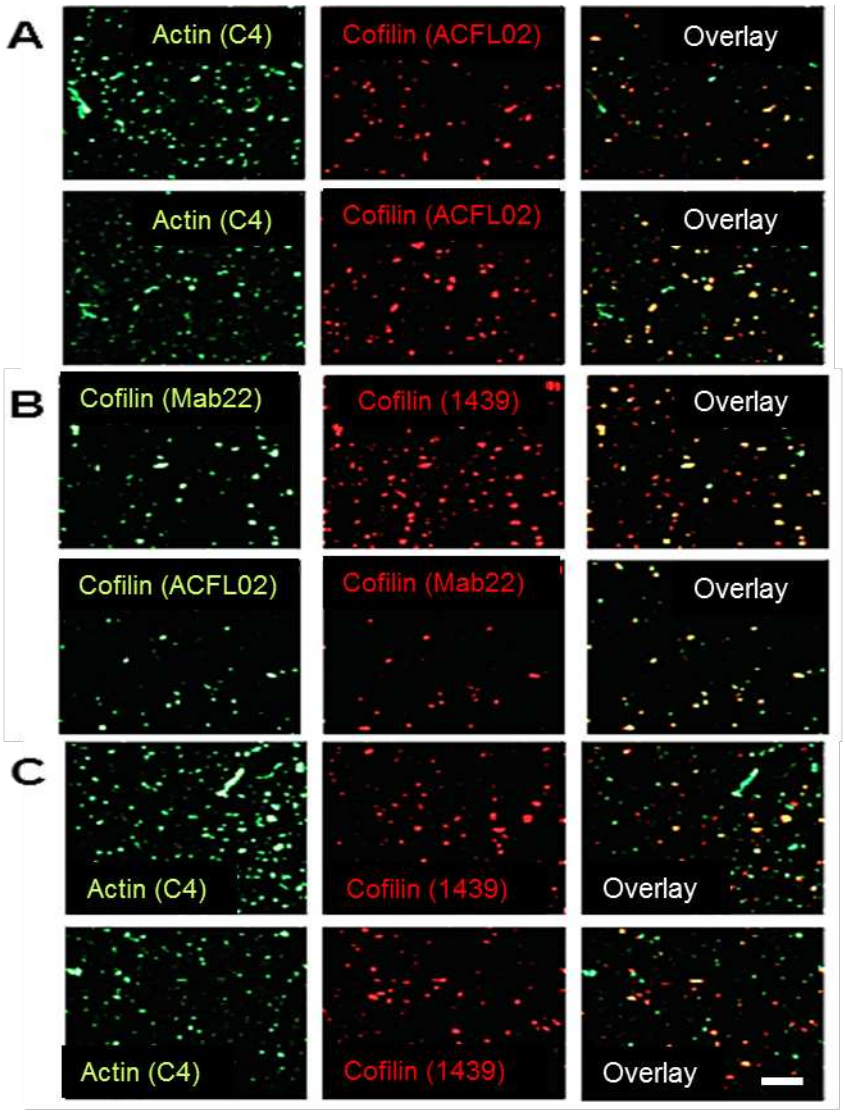

Figure 3.2 Specificity of antibody staining and rod composition. (**A** and **C**) Rods stained with a commercial cofilin antibody (ACFL-02) or rabbit 1439 antibody co-stain for actin, but not all actin staining structures co-stain for cofilin. (**B**) Co-staining of identical structures in the brain sections using the cofilin mouse monoclonal antibody MAb22 and rabbit antibody 1439 (top panels) and ACFL-02 and MAb22, lower panels. Bar = 5 µm. *Image courtesy of Laurie Minamide.*

All antibodies stained similar structures in different sections but staining intensity was quite dependent on the antibody and permeabilization protocol. For double labeling immunofluorescence the best permeabilization protocol utilized 80% methanol + 20% 1X PBS for 90 sec followed by 0.05% Triton-X 100 in 1x PBS for 90 sec. Two of the cofilin antibodies

were used to stain rods along with the actin monoclonal antibody, C4. Virtually all cofilin positive structures stained at variable intensities for actin but not all actin structures stained for cofilin.

Hippocampal analysis focused on five specific areas: the outer edge of the external plexiform layer (EPL), the pyramidal layer from CA1 to CA2 (CA Pyr), CA3, the subiculum (SUB), and layer 1 of the entorhinal cortex (ERC) (**Figure 3.3**).

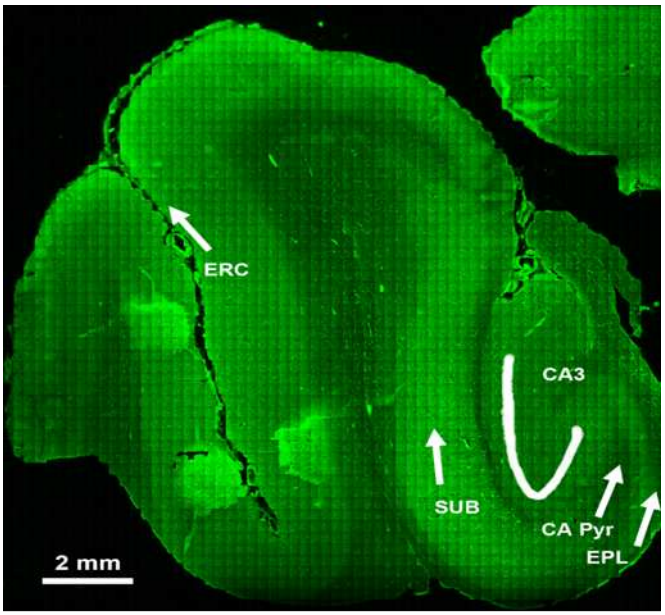

Figure 3.3 Regions of Interest in the Hippocampus. Montage of the hippocampal formation stained with 1439 (cofilin), scans taken with a 10X objective. Total scan area of hippocampal formation is equivalent of over 60,000 fields taken with a 60X objective. Rod and NT quantification was performed on 10 image stacks within each of the labeled regions. *Image courtesy of Laurie Minamide.*

Within each region, ten fields were captured for analysis with the 60X objective. Image stacks were obtained on the spinning disk confocal microscope that included at least one plane above and below the 30 μm thick slice to ensure the entire slice was imaged. A projection image was obtained for each image stack and this image was deconvolved using Metamorph software.

Rods were more prevalent within the ERC than in the other hippocampal areas. Rod quantification within the ERC showed a significant correlation with AD progression (**Figure 3.4**). Both rods and NT pathology increased significantly between NCI and eAD groups. Importantly, the median percent area of rod and NT pathology deposition was almost equivalent between the NCI and eAD groups. NT pathology in the ERC increased more in the mid to late AD subjects than did rods, but for two AD subjects rod pathology was equal to or greater than NT pathology. Thus rods may be an earlier indicator of AD progression than NT and possibly be equally important in disease progression in some subjects. Following the analysis within the Hippocampal formation, we then sought to conduct a similar study on frontal cortex tissue samples from nearly identical subject cohorts.

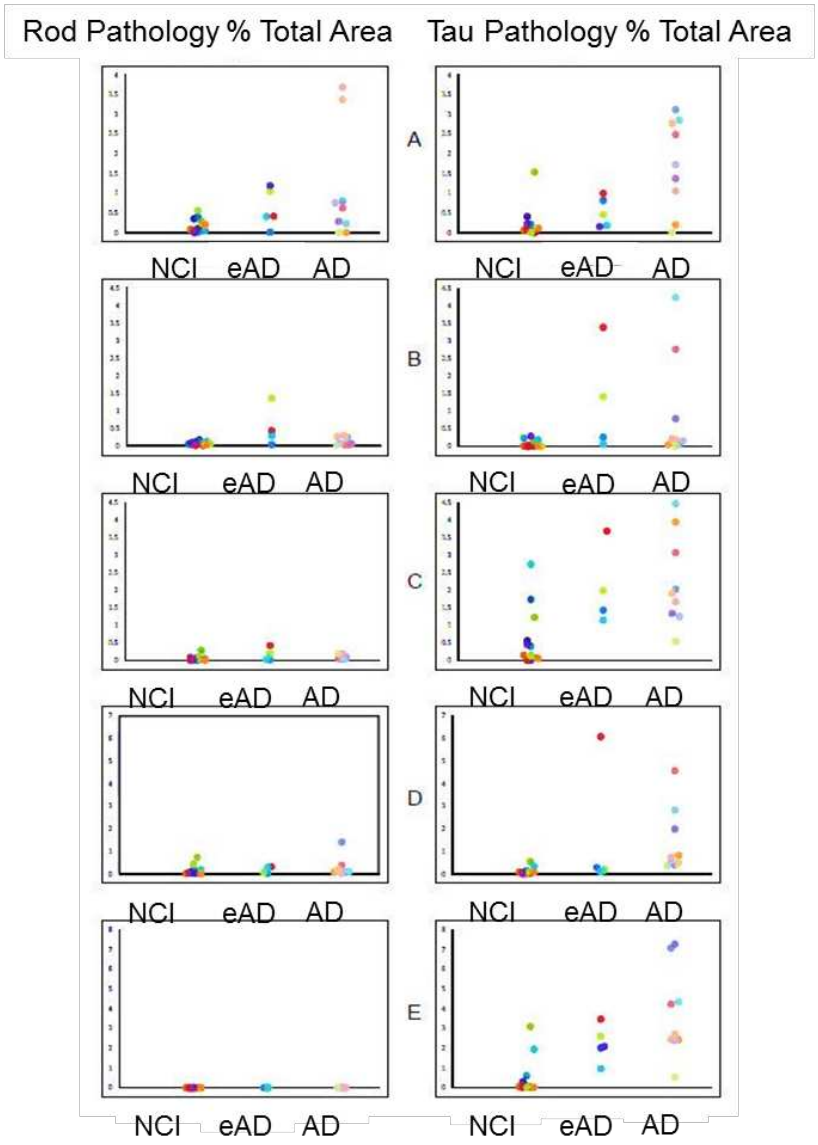

Figure 3.4 Rod and Tau Pathology Quantification within the Hippocampus. (Figure Regions: **A**. ERC, **B**. EPL, **C**. CA pyr, **D**. CA3, and **E**. Sub.) A direct comparison of cofilin-actin rod areas versus striated neuropil thread areas. Each individual is represented by a different colored dot, and the color represents the same individual on each graph. Each dot is an average of the 10 image stack % area deposition within each region. Rods remained low in the majority of regions (**B-E**), but appear to undergo significant disease transitional changes within the entorhinal cortex (**A**). Tau pathology in the NCI brain overall remained low (**A-E**), but was more variable than rod pathology. However, tau pathology did exhibit increasing median area deposition from NCI to AD across all areas. Importantly, the median percent area of rod and tau deposition in the entorhinal cortex (**A**) was nearly identical in NCI and eAD subjects. *Image courtesy of Laurie Minamide*

Frontal Cortex Tissue Analysis

Frontal cortex samples were received from the same subjects with the exception of 4 NCI subjects, giving us 8 NCI, 5 eAD and 9 AD subject groups for analysis. Initially, we used the same imaging strategy as we applied above for the hippocampal formation using 30 μm frozen sections. However, we quickly found that the frontal cortex samples lacked a defining physical morphology to allow identification of similar structural regions, so five imaging regions were chosen at random (**Figure 3.5**).

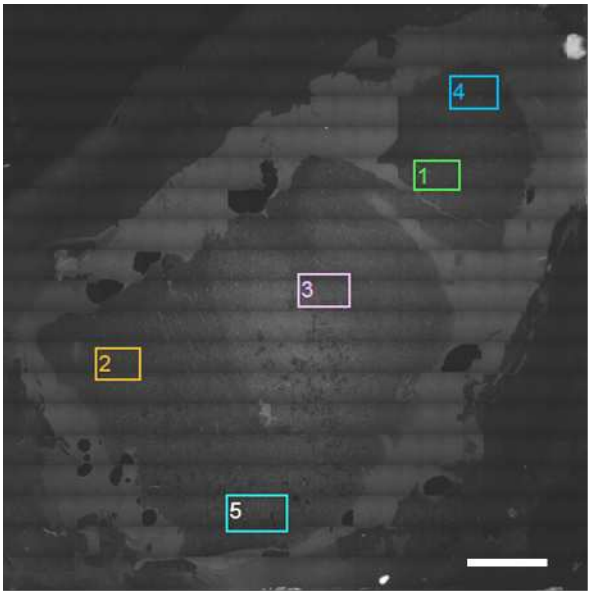

Figure 3.5 Initial Frontal Cortex Imaging Strategy. The lack of morphological landmarks within the sections of frontal cortex made it impossible to align regions between different samples. Thus, our initial imaging was performed by choosing 5 random fields across the section. Bar = 2 mm.

Within each of these regions, as within the hippocampus, 10 image stacks were taken and analyzed. Random densities of both rod and tau pathology were found across all individual

sample groupings and within each subject each of the 5 regions gave high variability. Thus it was clear that a new methodology was necessary to allow us to determine in what cortical layer we were imaging.

The standard method used to visualize cortical cell layers is Cresyl Violet staining (91, 92). We applied this staining to one frontal cortex slide and could readily visualize the 6 different layers (lamina) which define the morphology of the frontal cortex (**Figure 3.6**).

These layers are: the most external molecular layer (layer 1), external granular layer (layer 2), external pyramidal layer (layer 3), internal granular layer (layer 4), internal pyramidal layer (layer 5) and the most internal multiform layer (layer 6). Thus, we decided to image samples using the defined cortical layers for comparison across groups.

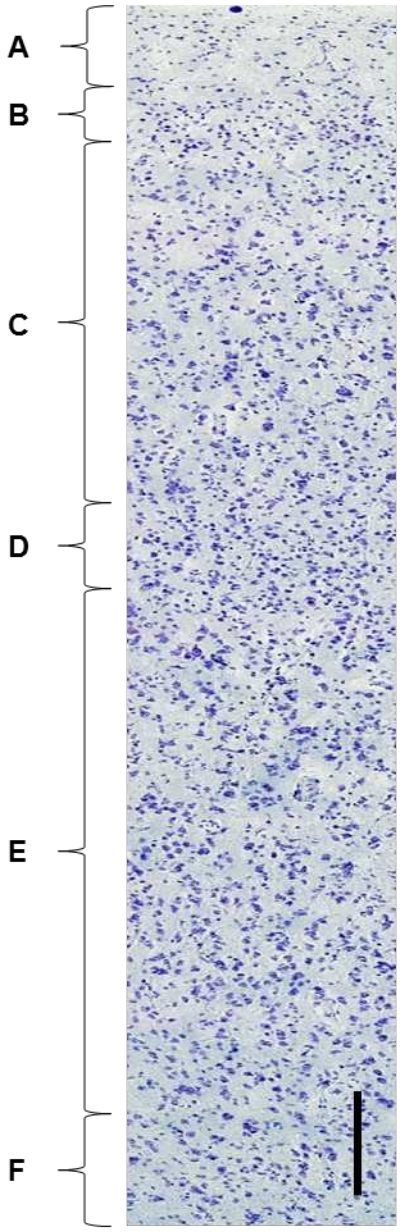

Figure 3.6 Lamina of the Frontal Cortex. A Cresyl Violet whole-cell stain of the frontal cortex tissue enabled us to differentiate the various cell layers (lamina) which were relatively uniform in their width around the cortical sections provided we could identify the external layer. (**A**) The external cortex begins with lamina 1 the (molecular layer), then (**B**) lamina 2 the (external granular layer), (**C**) lamina 3 (external pyramidal layer), (**D**) lamina 4 (internal granular layer), (**E**) lamina 5 internal pyramidal layer, (**F**) lamina 6 (internal multiform layer).

We initially started image acquisition using the spinning disk confocal microscope to obtain image stacks as with the hippocampus, attempting to obtain 5 image stacks starting in layer 1 and progressing inward (**Figure 3.7**).

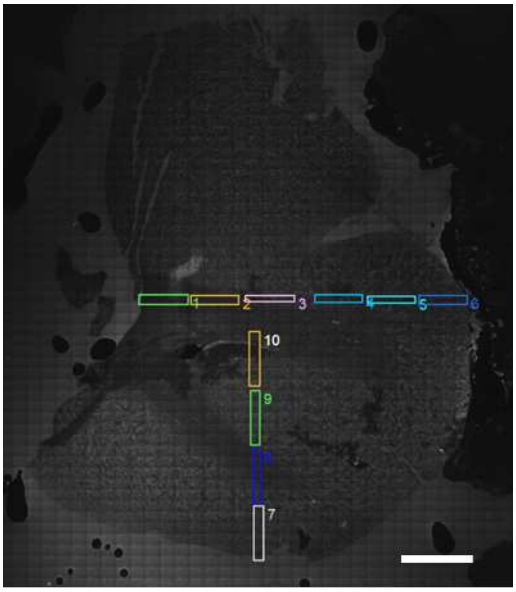

Figure 3.7 Imaging the Frontal Cortex following Cresyl Violet Staining. Knowing the location and relative thickness of the different cortical layers from the cresyl violet staining, different sections that were immunostained could be imaged with a new strategy. Within each cortical section we imaged 10 regions that covered all of the various layers as shown by the colored boxes. Bar = 2 mm.

However, in fluorescence imaging it was very difficult to know precisely in what region we were imaging, making the task extremely difficult and very slow. During this period CSU acquired an Olympus VS120 rapid scanning fluorescence microscope, housed at the Diagnostic Medical Center in the CSU Veterinary Teaching Hospital. This microscope is specifically designed for

semi-automated imaging large regions utilizes a 40x air objective and allowed us to image regions that were more than 67 times the areas quantified using the spinning disk microscope. We obtained full scans of the slice under low magnification and then imaged a 2.6 mm x 0.4 mm rectangle encompassing 1.04 mm^2 area which encompassed a region from the external cortex through to the internal cortex (**Figure 3.8 A**). Two of these rectangular images, generally at right angles to each other, were acquired for each sample (**Figure 3.8 A-C**). Images were processed and analyzed utilizing the same Metamorph software as was used for the hippocampal slices.

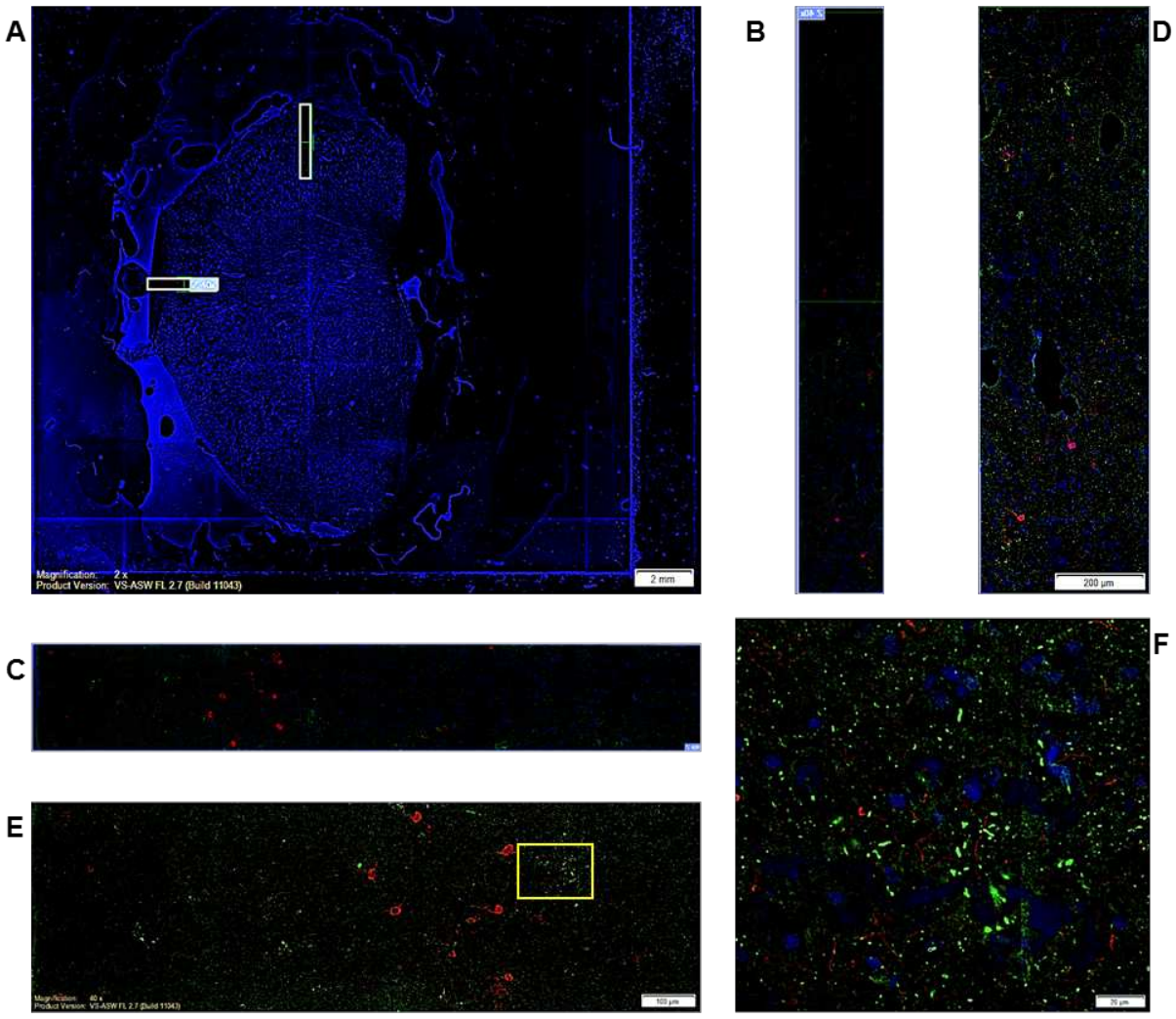

Figure 3.8 Imaging Frontal Cortex Sample with Olympus VS120 Scanning Microscope. Following the revised strategy for frontal cortex imaging, it was decided imaging was best conducted with the Olympus scanning microscope. (**A**) An initial scan of the whole tissue sample shown in DAPI, size bar 2mm. Within the whole-image scan, two rectangular scans of 2.6 mm x 0.4 mm are made as shown in A, with enlargement of each rectangle scan in (**B**) and (**C**). To process each image, they are cropped at 1.3mm (in half) and analyzed separately. (**D** and **E**) Cropped top-half images of B and C, respectively. D size bar 200 µm and E size bar 100 µm. (**F**) Enlarged image of region shown within yellow box in the outer cortex (Layer 3) at the magnification required for rod analysis, size bar 20 µm.

To verify the areas imaged within each sample represented the various cortical layers, we sought to Cresyl Violet stain and image previously immunostained sections (**Figure 3.9**).

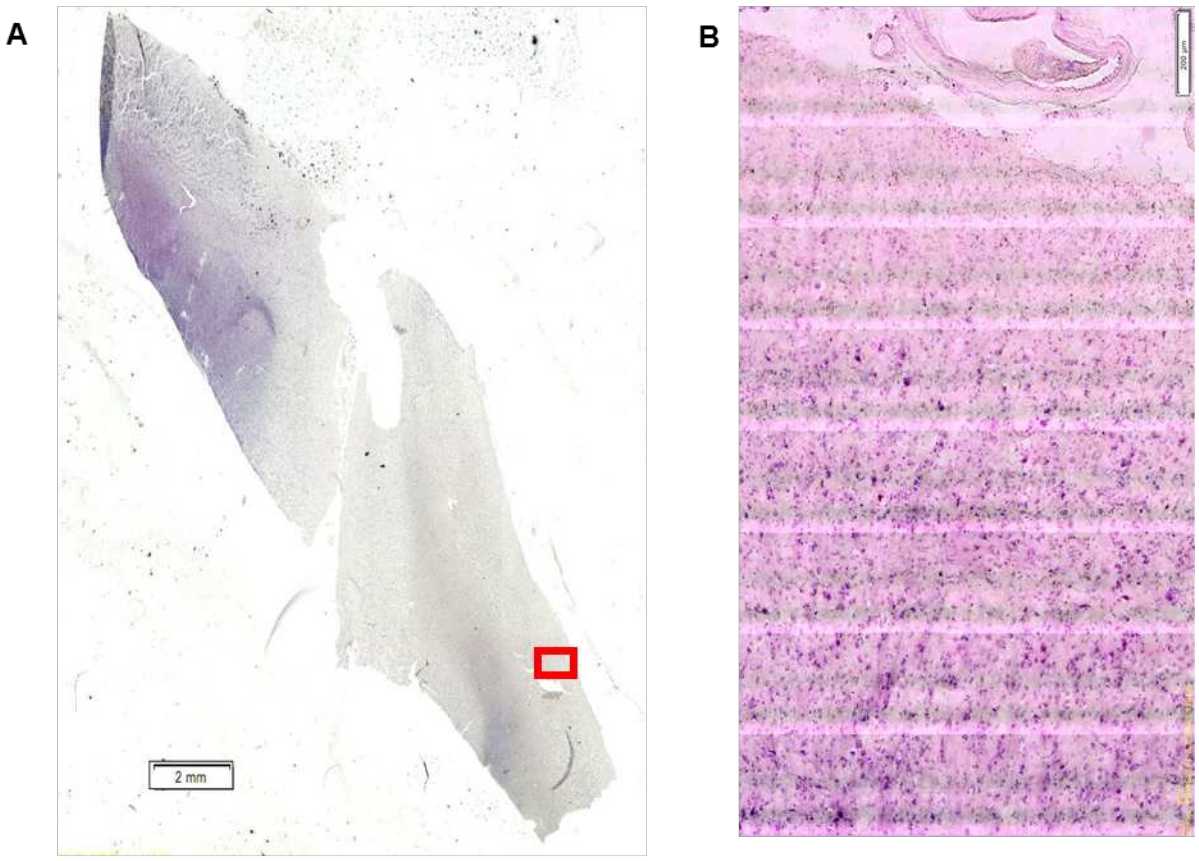

Figure 3.9 Cresyl Violet re-stain of previously immunostained samples. Upon observing the morphology of the lamina with the Cresyl Violet staining technique, we sought to extend the technique to previously immunostained and imaged samples. Cresyl Violet staining of imaged samples would allow us to verify all lamina were included within set 2.6 mm x 0.4 mm imaged areas. (**A**) An overview image of a re-stained Cresyl Violet sample with a 4X air objective, size bar 2 mm. The red box outlines the enlarged image shown in (**B**). (**B**) Image taken with 40X air objective of re-stained Cresyl Violet sample, size bar 200 µm.

To stain samples, the coverslips needed to be removed from ProLong Antifade Gold mounting medium. This was achieved by soaking the slides in 37° C water bath for two hours, letting them sit overnight and soaking again for another two hours. Following the incubations, the coverslips could be removed with slight mechanical manipulation. Once the coverslips were removed, the sections were able to be stained with Cresyl Violet using an extended incubation in the Cresyl Violet stain. The re-staining of previously imaged samples revealed greater variability in the thickness of the cortical lamina than we had previously appreciated. Thus, the 2.6 mm imaging depth did not adequately cover all 6 cortical lamina, but that layers 1-5 were covered for every

sample. We proceeded with our analysis since layer 6 is known to have a highly variable cell structure. Furthermore, significant disease pathology was previously shown to occur within layers 1-5, specifically layers 3 and 5 (84).

Cofilin staining appeared to vary throughout the cortical layers and we did not observe any significant differences in what we have identified as cofilin-stained “rod-like” puncta within any of the subject cohorts (**Figure 3.10**). On average, rod-like cofilin staining appeared in the frontal cortex, to a greater extent than what was observed in most areas of the hippocampal formation, with the exception of the ERC. Rod areas varied between 0.18-1.07% in NCI, 0.36-1.4% in eAD, and 0.04-1.2% in AD.

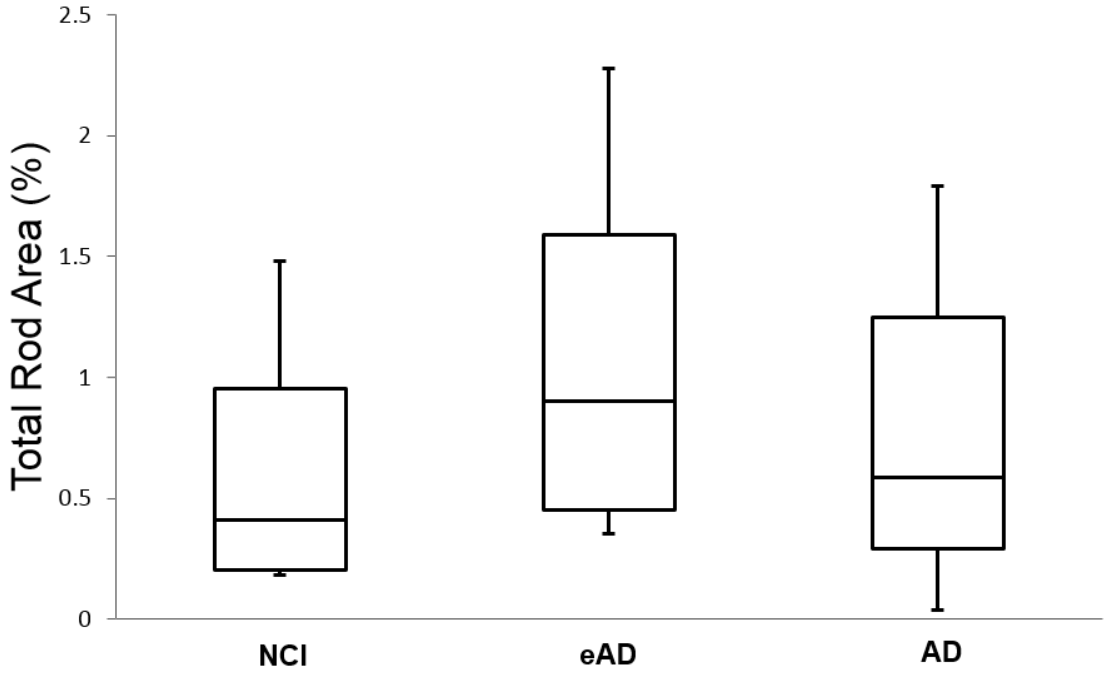

Figure 3.10 Rod Density within Frontal Cortex NCI, eAD and AD Subjects. The above box and whisker diagram represents the overall rod quantification data from NCI, eAD and AD subjects. The two 2.6 mm x 0.4 mm rectangle areas are averaged together for each sample. The median value of % rod area for each subject cohort is represented by the middle line through the box. The top and lower lines of each box represent the upper and lower quartiles of each cohort data set, respectively. The whiskers (lines) extending from each box represent the data range, maximum and minimum values within each data set. On average rods appear highly prevalent within the frontal cortex. Rod area ranged from 0.18 - 1.07% for NCI, 0.36 – 1.4% in eAD and 0.04 – 1.2% within the AD cohort. However, disease transition did not significantly correlate with rod density with p-values of 0.062 for NCI to eAD, 0.18 for NCI to AD, and 0.18 for eAD to AD.

Even when the rod quantification was separated between the inner 3 and outer 3 cortical layers, there was no correlation with disease progression (**Figure 3.11**).

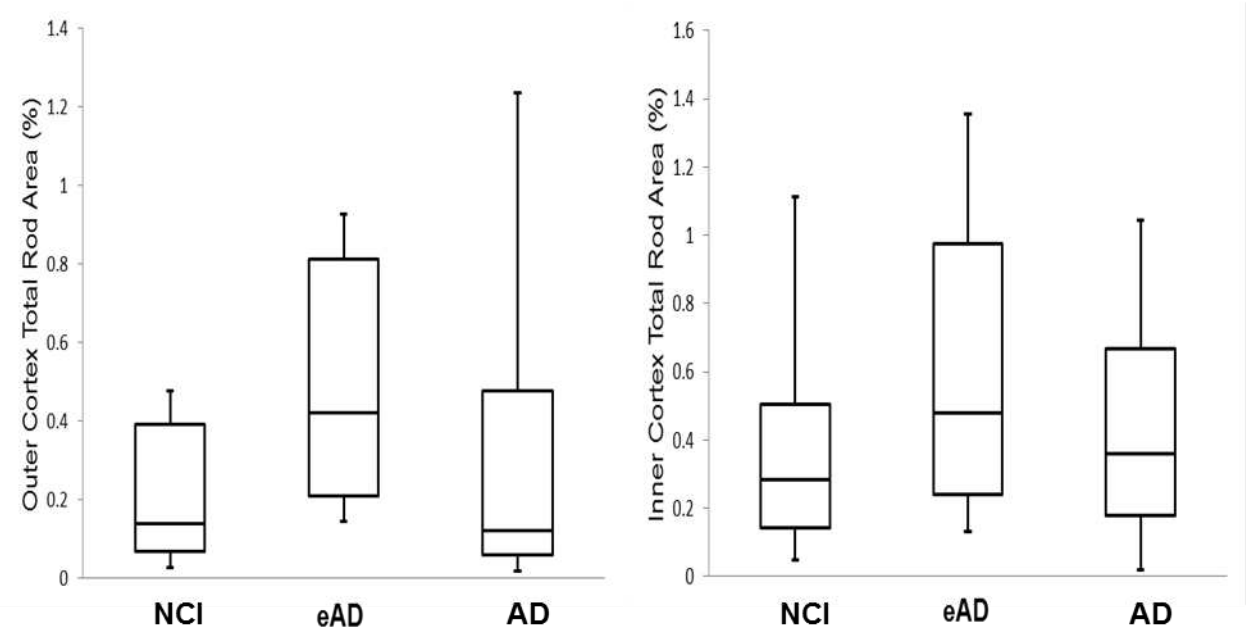

Figure 3.11 Frontal Cortex Rod Quantification in Outer and Inner Cortical Regions. Rod quantification was performed on the cortical outer layers (1-3) and inner layers (4-6), separately, but as with the total area, no significant differences existed between the NCI, eAD and AD subjects.

However, phosphorylated tau pathology showed a clear correlation with disease progression comparing both NCI to eAD and NCI to AD (**Figure 3.12**), with a median % total area phospho-tau deposition of 0.020% for NCI, 0.086% for eAD and 0.10% for AD. However, there was no significant increase in tau NT pathology between eAD and AD, but this may be a reflection of the small sample numbers of eAD brain that were available. Furthermore, when sections were separated into outer and inner cortex regions they continued to show a significant increase with disease transition between NCI to eAD and NCI to AD groupings, but again failed to show any significant increase with transition between eAD and AD (**Figure 3.13**). To confirm that the imaging data obtained on the Olympus microscope was consistent with data obtained by the

spinning disc confocal microscope, we compared similar sample areas between images obtained on the two systems. A similar rod density measured as % total area was found between images obtained from either microscope system (data not shown).

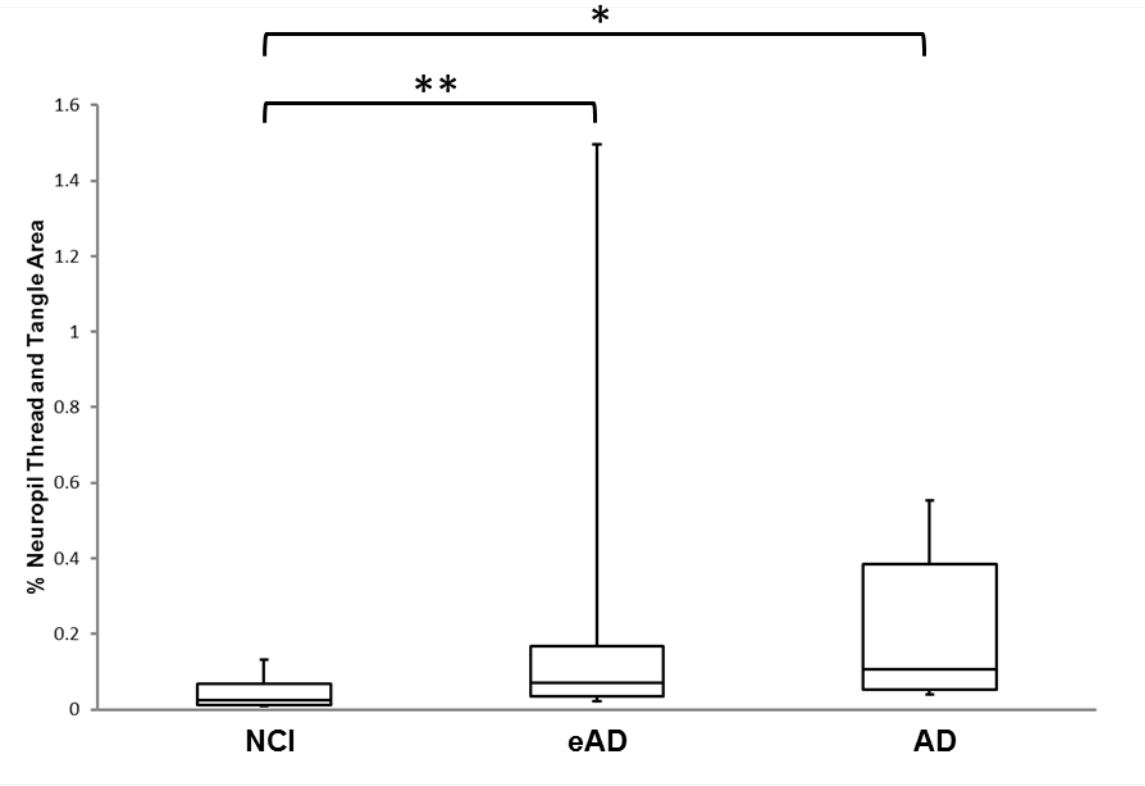

Figure 3.12 Neurofibrillary and Neuropil Tau Pathology Quantification within the Frontal Cortex. Within the frontal cortex, tau pathology does significantly correlate with disease progression in subjects from NCI to eAD (** p-value = 0.046) and NCI to AD (* p-value = 0.0040), but not eAD to AD (p-value = 0.21). Median % area of tau deposition was 0.020% in NCI, 0.086% in eAD, and 0.10% in AD. However, even at its highest point in AD, average tau pathology within the entire sampled region (0.1%) was far less than rod pathology (over 0.5%).

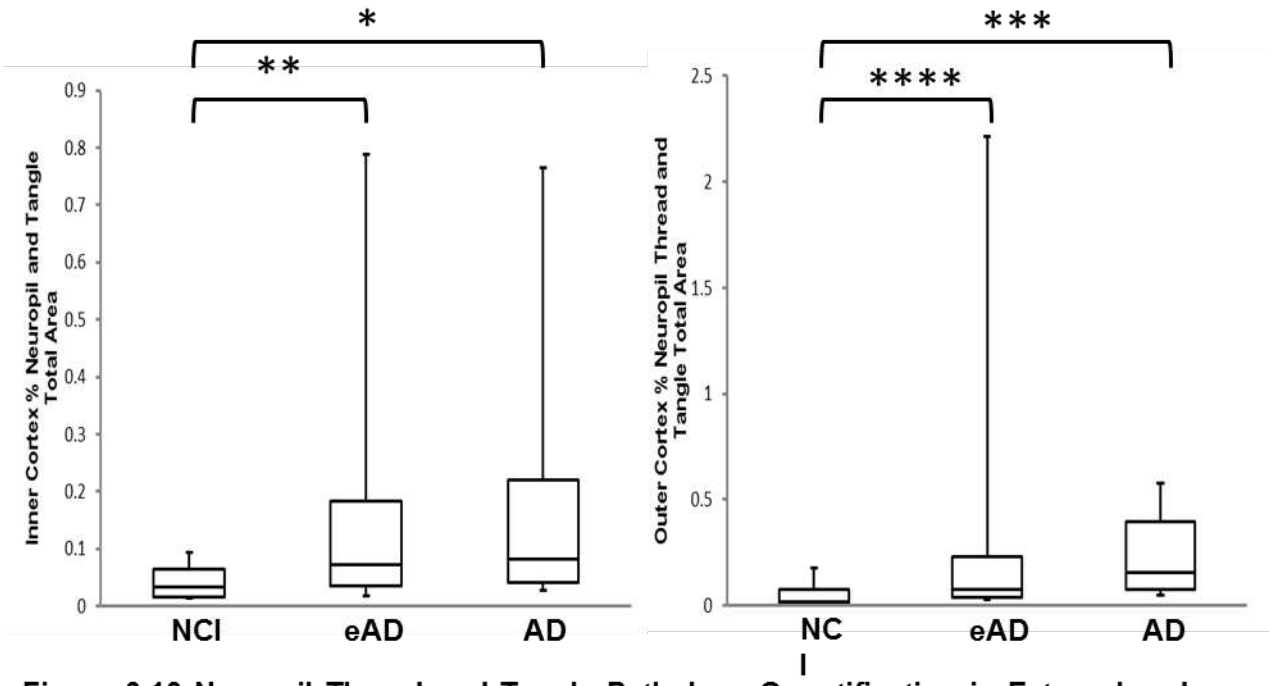

Figure 3.13 Neuropil Thread and Tangle Pathology Quantification in External and Internal Cortical Regions of the Frontal Cortex. When the quantification of tau pathology within the frontal cortex is separated into outer (layers 1-3) and inner (layers 4-6) cortical regions, they exhibit the similar significant disease correlations between NCI to eAD and NCI to AD subjects(* p-value = 0.0031, ** p-value = 0.046, *** p-value = 0.0054, **** p-value = 0.034).

Addendum 1

		Age at	Post-mortem	MMSE	Braak	CERAD
NCI	Gender	Death	interval (hrs)			
1187	F	84	2.5	28	0	0
1179	F	87	2.3	30	V	DEF
1200	F	92	3.2	30	III	PROB
1217	M	78	1.4	28	III	0
1216	F	79	1.8	29	I	0
1184	F	82	3	29	III	0
1190	F	101	3	26	IV	PROB
1203	F	85	2.8	30	III	POSS
eAD						
1201	M	94	2	22	V	PROB
1174	M	96	3.3	22	V	DEF
1172	F	85	2.75	23	IV	0
1202	F	80	3.3	22	VI	DEF
1195	M	98	2.5	24	II	PROB
AD						
1194	F	99	2	16	V	DEF
1185	F	79	2.9	10	VI	DEF
1169	F	93	2	5	V	DEF
1215	F	91	?	13	V	DEF
1204	F	72	2	2	VI	DEF
1168	F	80	4	16	VI	DEF
1199	M	88	2.7	11	VI	DEF

1197	**F**	**96**	**2.6**	**9**	**V**	**PROB**
1198	**F**	**92**	**3.6**	**19**	**V**	**DEF**

Chapter 4: Adenoviral NADPH Oxidase Probes

Introduction

Due to its high metabolic rate, the brain utilizes about 20% of the body's oxygen consumption at rest. To deal with the high production of reactive oxygen species (ROS) the brain has many REDOX mechanisms available but these systems decline with age. Evidence of oxidative stress has been correlated with neurodegenerative disease. Recent evidence indicates Aβ and proinflammatory cytokines, such as TNF-α, use a prion protein (PrP^C) dependent pathway to activate NADPH oxidase and induce rods (54). If PrP^C density is responsible for whether a rod forms, it would be beneficial to investigate the NOX intensity and duration of activity in relation to where rods form in a neurite. To accomplish this goal we developed the NOX probes p47-roGFP and NOX-2-RedTrack. Our observations indicate the p47-roGFP successfully localizes to the membrane with NOX activation and efficiently serves as a ROS biosensor. The NOX-2 RedTrack construct successfully expresses NOX-2 and mRFP fluorescence within mammalian cells.

P47-roGFP and NOX-2-RedTrack Construct Generation

The p47-roGFP and NOX-2-RedTrack probes were generated with the AdEasy adenoviral system for transgene expression within primary cultured neurons. To begin building our p47-roGFP construct, we received a p47-roGFP-pcDNA3.1 plasmid, which had previously been characterized for its ROS biosensing activity (93). For the NOX2-RedTrack construct we began with a NOX-2-pCMV6 plasmid with terminal FLAG and c-myc tags from Origene. To generate the constructs we performed multiple rounds of specific endonuclease cutting, band purification and splicing, and bacterial transformation to express the constructs in pShuttle vectors.

Specifically, for the RedTrack mRFP expression, the NOX-2-pCMV6 plasmid was subcloned into a RedTrack pShuttle, while still maintaining the NOX-2 FLAG and c-myc terminal tags. We then performed recombination of each construct with the pAdEasy backbone in E Coli BJ5183 cells, isolated and identified clones containing the recombined adenovirus constructs. We then transfected HEK293 cells separately with these clones, produced and amplified the virus. A viral titer assay was performed, the p47-roGFP stock contained 2.5 x 10^9 infectious particles, while the NOX-2-RedTrack stock contained 1.6 x 10^{10} infectious particles.

P47-roGFP and NOX-2-RedTrack Construct Characterization

To confirm the expression of the p47-roGFP and NOX-2-RedTrack constructs we performed western blot analysis (**Figure 4.1**). N2a cells, a fast-growing mouse neuroblastoma cell line were infected with the adenovirus constructs. When the majority (greater than 50%) of cells exhibited fluorescence (about 48 hr postinfection), they were washed and lysed utilizing as SDS-lysis buffer. The western blot was performed against the GFP protein (**Figure 4.1 A**), FLAG and c-myc tags (**Figure 4.1 B**) and cofilin as a standard control (**Figure 4.1 A and B**). In Figure 4.1 A the appearance of the positive p47-roGFP band at 70 kDa in p47-roGFP infected cells but not NOX-2-RedTrack infected or uninfected cells confirmed expression of p47-roGFP. In Figure 4.1 B, a positive NOX-2 band at 65 kDa in NOX-2-RedTrack infected cells, but not p47-roGFP infected or uninfected cells confirmed successful NOX-2 expression from the NOX-2-RedTrack construct.

To confirm RFP expression of NOX-2-RedTrack, human Hela cells were infected with the NOX-2-RedTrack adenovirus and imaged with a 60X objective on a spinning-disk confocal microscope. RFP expression was positively identified with infected cells emitting bright red light

when excited with a 561 nm laser (**Figure 4.2**), while uninfected cells emitted no light when excited with the 561 nm laser.

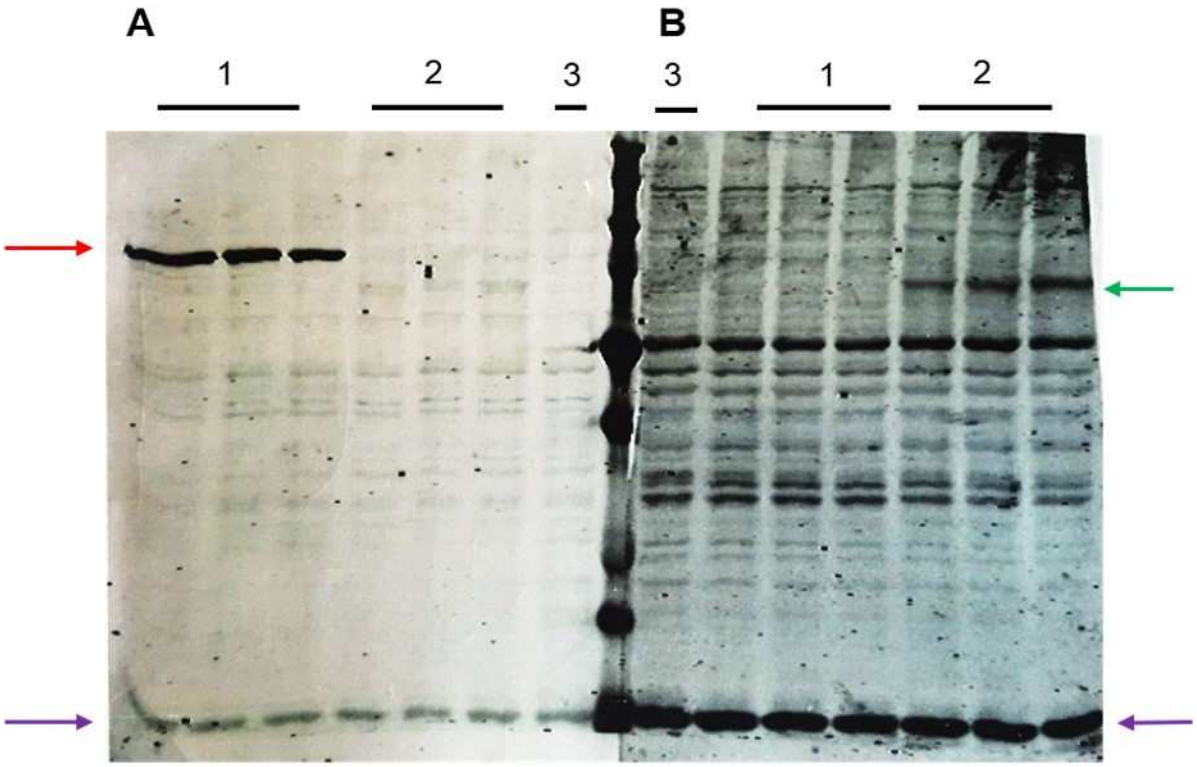

Figure 4.1 Western Blot Analysis. Western blot analysis of p47-roGFP and NOX-2-redtrack adenoviral constructs. Western blot performed using cell extracts from infected and uninfected mouse neuroblastoma (N2a) cells. Lane 1 is a cell extract from p47-roGFP infected cells, lane 2 is cell extract from NOX-2-redtrack infected cells, and lane 3 is cell extract from uninfected cells. (**A**) Blot against GFP and cofilin as a standard control. There is a positive p47-roGFP band in infected cells only at 70 kDa indicated with the red arrow. The standard control cofilin band is present in all cell extracts at 17 kDa indicated with the purple arrow. (**B**) Blot against FLAG, c-myc and cofilin as the standard control. There is a positive NOX-2 band in NOX-2-redtrack infected cells only at 65 kDa indicated by the green arrow. The standard control cofilin band is present in all cell extracts at 17 kDa indicated by the purple arrow.

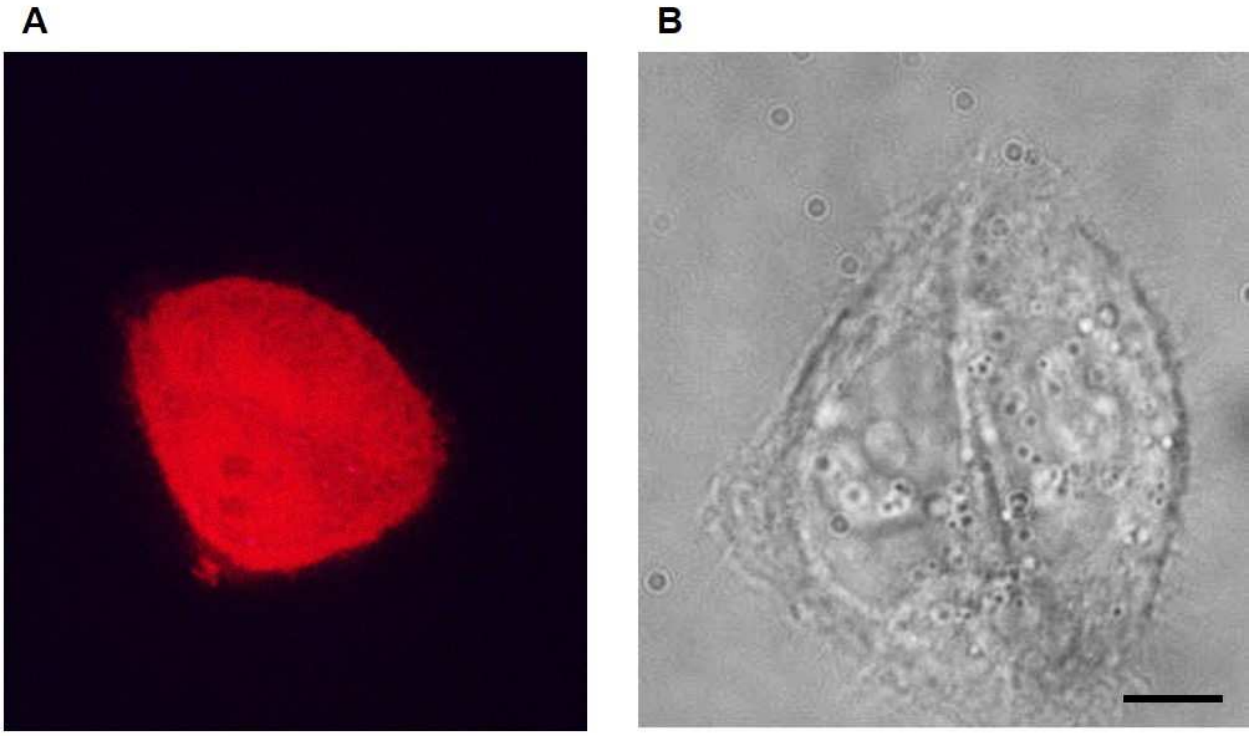

Figure 4.2 Redtrack RFP Expression in Hela Cells. Hela cells infected with NOX-2-redtrack adenovirus. Images taken with 60X objective of spinning-disk confocal microscope. Images are the same cell, but are rotated with respect to one another. (**A**) Hela cell excited with 561 nm light indicating positive RFP expression from NOX-2-redtrack infected cell. (**B**) Bright-field (DIC) image of infected cell in A. Infected cell appears healthy. Bar = 10 mm.

The localization and activity of adenoviral expressed p47-roGFP was characterized in by Keifer Walsh. Characterization was performed in primary rat hippocampal neurons infected with the p47-roGFP adenovirus. Neurons were imaged on a Nikon Eclipse 2000 inverted TIRF microscope with the 60X objective using 405 nm and 488 nm lasers. To measure the ROS by roGFP, a ratio of 405 nm to 488 nm (405/488) normalized fluorescence intensity is taken. When ROS species are generated, a decrease of 488 nm fluorescence intensity is observed, contributing to an increase in normalized fluorescence of the 405/488 ratio. When neurons are treated with hydrogen peroxide (H_2O_2) a form of ROS, an increase in the ratio of normalized fluorescence intensity is observed throughout the cell (**Figure 4.3**).

Conversely, when the neurons are treated with N-Acetyl-Cysteine (NAC) an antioxidant, a decrease in the ratio of normalized fluorescence intensity is observed. The observations indicate the p47-roGFP construct is properly sensing changes of ROS levels in vivo. To determine the localization and activation of p47-roGFP, primary rat hippocampal neurons were treated with the NOX-2 activating proinflammatory cytokine TNF-α (**Figure 4.4**).

As mentioned previously, the p47 NOX-2 subunit exists in the cytosol when not phosphorylated, but when activated p47 is phosphorylated and translocates to the membrane to associate with NOX-2. The proinflammatory cytokine TNF-α activates NOX-2, causing p47 membrane translocation. Initially, before TNF-α treatment, p47roGFP is diffuse within the cell (**Figure 4.3 A**) but 15 and 30 minutes after TNF-α treatment the p47roGFP fluorescence is concentrated at the membrane. In addition to exhibiting ROS sensitivity, the p47-roGFP adenovirus exhibits proper membrane translocation in vivo.

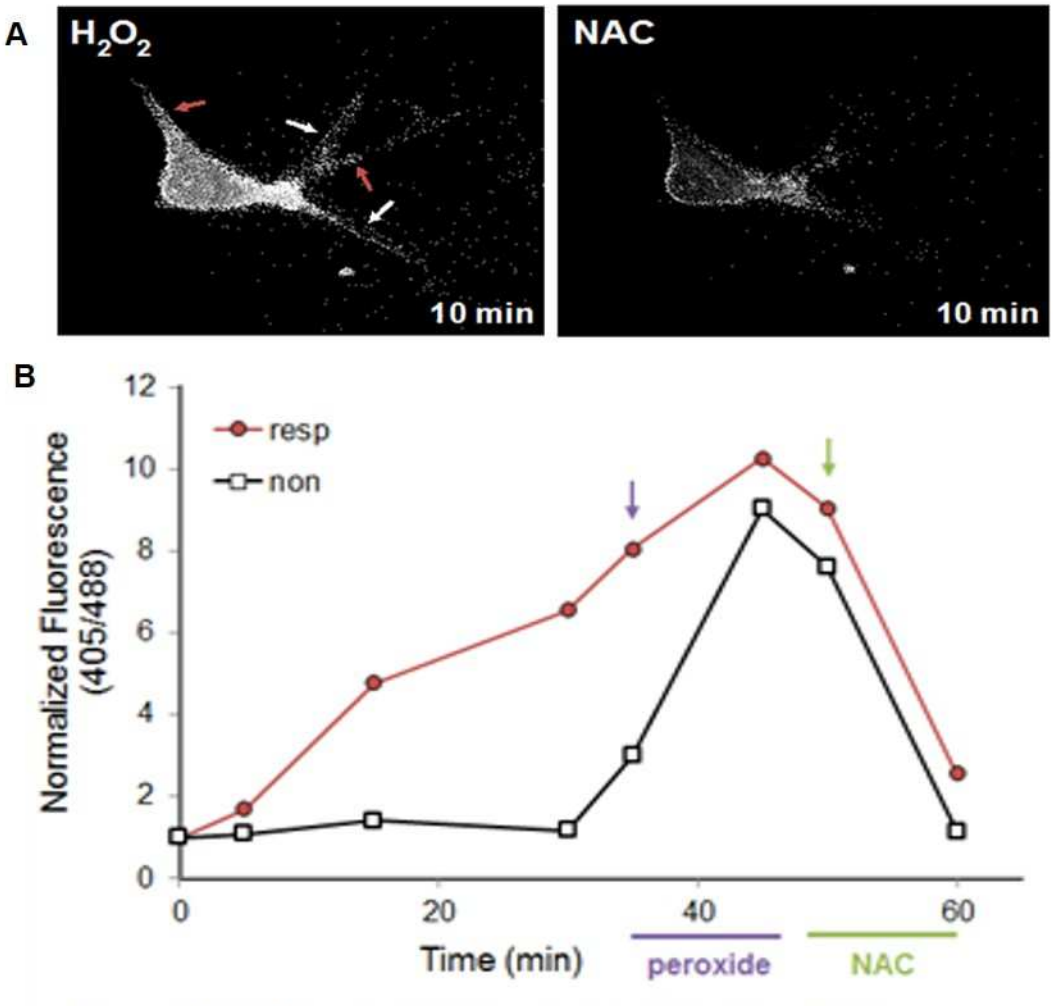

Figure 4.3 ROS Sensing Activity of p47-roGFP. When ROS is generated a increase in the ratio of 405/488 normalized fluorescence is observed. (A) Primary rat hippocampal neurons infected with p47-roGFP imaged with a 60X objective. When cells are treated with hydrogen peroxide (H_2O_2) an increase in the ratio 405/488 normalized fluorescence is observed. Conversely, when treated with the antioxidant N-Acetyl-Cysteine (NAC), there is a loss in ratio 405/488 normalized fluorescence. The decrease in fluorescence makes previously visible neurites (white and red arrows) all but invisible after NAC treatment. (B) Normalized fluorescence response to treatment of positively infected neurons (red line) and uninfected neurons (black line). Quantitative analysis of the ratio 405/488 of normalized fluorescence reveals increased fluorescent intensity following H_2O_2 treatment (purple arrow) and decreased intensity following NAC antioxidant treatment (green arrow). *Keifer Walsh, 2014.*

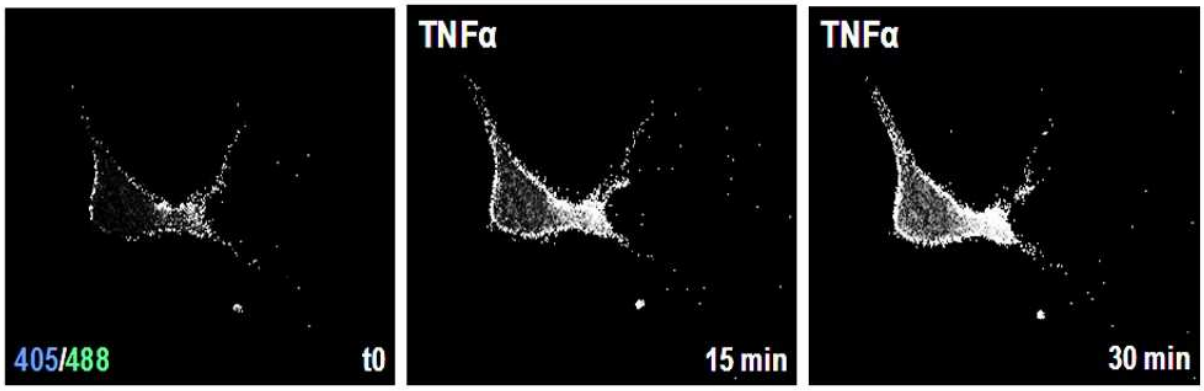

Figure 4.4 p47-roGFP Infected Cells Exhibit Membrane Translocation When Activated. Primary rat hippocampal neurons infected with p47-roGFP and imaged with a 60X objective. Cells are excited with both 405 nm and 488 nm light. Images are a ratio of 405/488 normalized fluorescence intensity. Before treatment t0, p47-roGFP is inactive in the cytosol. When treated with TNF-α, p47-roGFP becomes active and translocates to the membrane. Following 15 and 30 minutes of treatment, an increase in the membrane fluorescence intensity is observed, indicating p47-roGFP translocation to the membrane. *Keifer Walsh, 2014*.

Chapter 5: Discussion and Future Directions

Cofilin-actin rods are an easily induced pathological change in neurons. Rods have been characterized to form within the neurites, sequestering the majority of cofilin and growing to completely occlude the neurite. They are also induced in organotypic slice cultures of hippocampus and are not present prior to their induction by agents that are thought to induce synaptic deficits or neurodegenerative disorders. Rods have a distinct composition and have been made in vitro from just actin and cofilin. When isolated from neurons, rods contain 1:1 cofilin:actin and thus are probably cofilin-saturated filaments that bundle when subjected to oxidative cross-linking. They show the parallel array of filaments when examined by transmission electron microscopy, and they are composed of variable filament lengths when quantified by EM tomography. Rod formation in cultured neurons is easily followed with fluorescent probes and these rods immunostain for cofilin and actin. However, defining exactly what constitutes a rod or an aggregate by cofilin immunostaining within fixed brain tissue is much harder to establish. Cofilin is an essential component of dendritic spines, so all punctate cofilin immunostaining observed in the brain may not arise from rods.

Thus, our initial efforts aimed to establish what we defined as a rod based upon cofilin and actin immunostaining. We were guided by certain characteristic features of rods that have been observed. From previous work we knew rods had a specific size range of 2-10 μm in length, while they also did not exhibit any curvature. Additionally, rods should co-stain for actin. Following these parameters, we decided to utilize a pixel size of 4-50 for rods. Although some images showed a higher background staining (autofluorescence) than others, we utilized a constant background intensity for all of the sections, knowingly excluding some stained

structures that were probably rods from some of the analysis rather than incorporating some autofluorescent material.

Immunostainings for rods or aggregates in the hippocampus of short postmortem interval brain samples from subjects in a longitudinal study showed very little cofilin pathology in the entorhinal cortex (ERC) of non-cognitively impaired subjects, increasing slightly in early AD and increasing more dramatically in AD, especially within a subcohort of subjects. It is not unexpected to see subjects with advanced AD that show no cofilin pathology in the limited brain areas explored, since even tau pathology, which is highly correlated with cognitive loss in AD, is not found in 10 fields of some of the subjects examined here. Other regions of the hippocampus that were examined in detail show less cofilin pathology than the ERC, which is the first brain region to exhibit AD pathology scored by traditional staining for plaques and tangles. Cofilin rod pathology and tau pathology do not overlap, a finding that supports the observations of Rahman et al (66) which were done across more brain regions but not in as great a detail as performed here. Rahman et al suggested cofilin pathology as being downstream of tau pathology, but our observations of increased rod pathology in the ERC of eAD subjects may implicate rods as an earlier pathology during AD development.

The human frontal cortex serves many roles which are susceptible to disruption within the context of AD. Indeed it is the preservation of function within a cholinergic pathway in the frontal cortex that is the target of the AD drug Aricept, an acetylcholinersterase inhibitor. Thus, we were surprised to find that the area of rods within the frontal cortex of NCI subjects was relatively high compared to most hippocampal brain regions and that it did not change significantly during disease progression. While these findings may suggest that rods do not play a significant role in

disease pathology within this brain region, the issue of rods in the frontal cortex may not yet be fully resolved. The greatest concern with rod quantification in the frontal cortex may be inclusion of non-rod structures in the quantification. Because we observe high levels of rod pathology within the frontal cortex across all NCI, eAD and AD classifications, it may be possible that some cofilin-immunostained structure, such as dendritic spines, may be contributing to the rod area. Thus we should perform at least some TEM cofilin-immunolabeling to identify ultrastructurally whether these structures have the typical rod bundle organization. Alternatively, the application of some newer imaging methods may be of help. Currently, one of these methods is CLARITY (94) which offers the unique advantage of multiple rounds of staining and imaging on a single sample. This could be quite advantageous within the frontal cortex where analysis of various structural markers could help to further differentiate the morphology of the frontal cortex, identification of spines, and improve the accuracy of rod quantification. However, this method is not without its own challenges which need to be overcome to successfully and consistently stain and image human postmortem brain tissue samples.

If the cofilin-immunostained structures in frontal cortex do turn out to be rods, we have already ruled out some of the sample-related variabilities that might account for them. We analyzed the samples for rods comparing postmortem time intervals, or subject age but neither of these showed any correlation with differences in rod areas. With our observation of the high rod density in the frontal cortex, future study will help determine if our results are immunostaining other cofilin structures or the possible indication rods may function in the frontal cortex in a previously unknown manner.

The influence of oxidative stress within the AD brain is significant, and may be important to better understanding of the disease process. Rods are highly susceptible to this oxidative stress, and there is early evidence indicating a possible rod inducing pathway which is dependent on the ROS generating NADPH oxidase. Here, we focused on establishing the foundation for future NOX study. We successfully developed the p47-roGFP and NOX-2-RedTrack probes, while confirming the activity and localization of p47-roGFP and the expression of NOX-2 and mRFP in cells infected with the RedTrack virus.

The successful generation of p47-roGFP acting as expected in neuronal cells will enable its use as a future tool to explore both oxidative conditions and NOX activity as they relate to rod formation. However, the need to ratio images with 405 nm light may limit the use p47-roGFP as a neuronal cell probe. Successive 405 nm exposure to neurons will induce additional toxic cell responses which will be difficult to account for using the p47-roGFP probe. However, the successful generation of the NOX-2-RedTrack probe will enable NOX overexpression studies to be done and determine the resulting rod response. With evidence that rods are induced via a NOX dependent pathway, we would not expect overexpression of NOX alone to induce rods. This is due to the lack of NOX activating factors such as Aβ or TNF-α. However, if NOX overexpression with Aβ or TNF-α treatment induces a greater rod response there is additional evidence of a NOX-dependent rod induction pathway which may correlate more directly with both NOX activity and expression.

The incidence of AD cases will only increase in the future. The sporadic nature of AD makes it difficult to track and analyze the underlying initiators of disease pathology. The effect of Aβ in early disease initiation may be widely accepted, but understanding its pathological action is

more controversial. It may elicit toxicity in a multi-factorial effect through oxidative stress, activation of neuronal immune cells, and tau pathology. Rods continue to show an evidence of induction in each of these pathways possibly providing a link to downstream Aβ induced toxicities. Further study is needed to understand how rods may be implicated AD, and if they warrant status as a therapeutic target.

References

1. "2015 Alzheimer's Disease Facts and Figures." *Alzheimer's and Dementia*. Alzheimer's Association. 2015, 11(3); 332.

2. Hebert LE, Becket LA, Scherr PA, Evans DA. " Annual incidence of Alzheimer disease in the United States projected to the years 2000 through 2050." *Alzheimer Dis Assoc Discord*. 2001, 15(4): 169-173.

3. Vinters HV. "Emerging Concepts in Alzheimer's Disease." *Annu. Rev. Pathol*. Mech DIs. 2015 10; 291-319.

4. Coyle JT, Price DL, DeLong MR. "Alzheimer's Disease: A Disorder of Cortical Cholinergic Innervation." *Science*. 1983, 219; 1184-1190.

5. Davies P and Maloney AJF. "Selective Loss of Central Cholinergic Neurons in Alzheimer's Disease." *Lancet.* 1976, 308(8000); 1403.

6. Bartus RT, Dean III RL, Beer B, Lippa AS. "The Cholinergic Hypothesis of Geriatric Memory Dysfunction." *Science*. 1982, 217; 408-416.

7. Corbett A, Pickett J, burns A, Corcoran J, Dunnett SB, Edison P, Hagan JJ, Holmes C, Jones E, Katona C, Kearns I, Kehoe P, Mudher A, Passmore A, Shepherd N, Walsh F, Ballard C. "Drug repositioning for Alzheimer's disease." *Nature*. 2012 11(11); 833-846.

8. Tiraboschi P, Hansen LA, Alford M, Masiliah E, Thal LJ, Corey-Bloom J. "The decline in synapses and cholinergic activity is asynchronous in Alzheimer's disease." *Neurology*. 2000 55 (9); 1278-1283.

9. Khan UA, Liu L, Provenzano FA, Berman DE, Profaci CP, Sloan R, Mayeux R, Duff KE, Small SA. "Molecular drivers and cortical spread of lateral entorhinal cortex dysfunction in preclinical Alzheimer's disease." *Nature Neuroscience*. 2014, 17(2); 304-313.

10. Brettschneider J, Del Tradici K, Lee VMY, Trojanowski JQ. "Spreading of pathology in neurodegnerative diseases: a focus on human studies." *Nature Rev. Neuro*. 2015, 16; 109-120.

11. Mueller SG, Schuff N, Yaffe K, Madison C, Miller B, Weiner MW. "Hippocampal Atrophy Patterns in Mild Cognitive Impairment and Alzheimer's Disease." *Hum Brain Mapp*. 2010, 31(9); 1339-1347.

12. Uylings HBM and Brabander JM. "Neuronal Changes in Normal Human Aging and Alzheimer's Disease." *Brain and Cognition*. 2002, 49; 268-276.

13. Small DH and Cappai R. "Alois Alzheimer and Alzheimer's disease a centennial perspective." *J of Neurochemistry*. 2006, 99; 708-710.

14. McKhann GM et al. "The diagnosis of dementia due to Alzheimer's disease: Recommendations from the National Institute on Aging-Alzheimers Association workgroup diagnostic guidelines for Alzheimer's disease." *Alzheimers Dement*. 2011 7(3); 263-269.

15. Hardy JA and Higgins GA. “Alzheimer’s Disease: The Amyloid Cascade Hypothesis.” *Science*. 1992 184; 184-185.

16. Kant R and Goldstein L. “Cellular Functions of the Amyloid Precursor Protein from Development to Dementia.” *Developmental Cell*. 2015, 32; 502-515.

17. Heppner FL, Ransohoff RM, Becher B. “Immune attack: the role of inflammation in Alzheimer disease.” *Nature Reviews Neuroscience*. 2015, 16; 358-372.

18. Hook V, Funkelstein L, Wegrzyn J, Bark S, Kindy M, Hook G. “Cysteine Cathepsins in the secretory vesicle produce active peptides: Cathepsin L generates peptide neurotransmitters and cathepsin B produces beta-amyloid of Alzheimer’s disease.” *Biochem Biophys Acta*. 2012, 1824(1); 89-104.

19. Herrup Karl. “The case for rejecting the amyloid cascade hypothesis.” Nature *Neuroscience*. 18 (6); 794-799.

20. Jarrett JT, Berger EP, and Lansbury PT Jr. “The carboxy terminus of the beta amyloid protein is critical for the seeding of amyloid formation: implications for the pathogenesis of Alzheimer’s disease.” *Biochemistry*. 1993, 32; 4693-4697.

21. Ballatore C, Lee VMY, Trojanowski JQ. “Tau-mediated neurodegeneration in Alzheimer’s disease and related disorders.” *Nature*. 2007, 8; 663-670.

22. Mazanetz MP and FIscher PM. “Untangling tau hyperphosphorylation in drug desing for neurodegernative diseases.” *Nature Rev. Drug Discov*. 2007, 6; 464-479.

23. Mohamed NV, Herrou T, Plouffe V, Piperno N, Leclerc N. “Spreading of tau pathology in Alzheimer's disease by cell-to-cell transmission.” *Eur J Neurosci*. 2013, 37; 1939-1948.

24. Tang Z, Ioja E, Bereczki E, Hultenby K, Li C, Guan Z, Winblad B, Pei J-J. “mTor mediates tau localization and secretion: implication for Alzheimer's disease.” *Biochem Biophys Acta*. 2015, 1853; 1646-1657.

25. Hashimoto, Tadafumi, et al. “Apolipoprotein E, Especially Apolipoprotein E4, Increases the Oligomerization of Amyloid β Peptide.” *The Journal of Neuroscience*. 32(43); 15181-15192. 24 October 2012.

26. Jones PB, Adams KW, Rozkalne A, Spire-Jones TL, Hshieh TT, Hashimoto T. et al. “Apolipoprotein E: isoform specific differences in tertiary structure and interaction with amyloid-beta in human Alzheimer brain.” *PLoS One*. 2011, 6;e14586.

27. Hardy J and Selkoe DJ. “The Amyloid Hypothesis of Alzheimer’s Disease: Progress and Problems on the road to therapeutics.” *Science*. 2002, 297 (19); 353-356.

28. Helmuth L. “Detangling Alzheimer’s Disease.” *Sci Aging Knowledge Environ*. 2001, 1; oa2.

29. Musiek ES and Holtzman DM. “Three dimensions of the Amyloid hypothesis: time, space and ‘wingmen’.” *Nature Neuroscience*. 2015, 18(6); 800-

30. Hardy, John. “Has the Amyloid Cascade Hypothesis for Alzheimer’s Disease been Proved?” *Current Alz Research*. 2006, 3; 71-73.

31. Selkoe DJ. “Alzheimer’s Disease Is a Synaptic Failure.” *Science*. 2002, 298; 789-791.

32. Puzzo D and Arancio O. “Amyloid-Beta peptide: Dr. Jekyll or Mr. Hyde?” *J Alzheimer’s Dis*. 2013, 33(1); 111-120.

33. Cleary JP, Walsh DM, Hofmeister JJ, Shankar GM, Kuskowski MA, Selkoe DJ, Ashe KH. “Natureal oligomers of the amyloid-beta protein specifically disrupt cognitive function.” *Nature Neuroscience*. 2004, 8(1); 79-84.

34. Frost B, Gotz J, Feany MB. “Connecting the dots between tau dysfunction and neurodegenration.” *Cell*. 2015, 25(1); 46-52.

35. Riedl L, Mackenzie IR, Forstl H, Kurz A, Diehl-Schmid J. “Frontotemporal lobar degeneration: current perspectives.” *Neuropsychiatric Disease and Treatment*. 2014, 10; 297-310

36. Oddo S, Caccoamo A, Lambert MP, Glabe CG, Klein WL, LaFerla FM. “ Temporal profile of amyloid-beta (Abeta) oligomerization in an in vivo model of Alzheimer disease. A link between Abeta and tau pathology.” *J Biol Chem*. 2006, 281 (3); 1599-1604.

37. Blurton-Jones M and LaFerla FM. “Pathways by Which Abeta facilitates Tau Pathology.” *Current Alzheimer Research*. 2006, 3(5); 437-448.

38. Cichon J, Sun C, Chen B, Chen XA, Sun Y, Wang Y, Chen G. “Cofilin Aggregation Blocks Intracellular Trafficking and Induces Synaptic Loss in Hippocampal Neurons.” *J Biol Chem*. 2012, 287(6); 3919-3929.

39. Bamburg JR, Bernstein BW, Davis RC, Flynn KC, Goldsbury C, Jensen JR, Maloney MT, Marsden IT, Minamide LS, Pak CW, Shaw AE, Whiteman I, Wiggan O. “ADF/Cofilin-Actin Rods in Neurodegenerative Diseases.” *Current Alzheimer Research*. 2010, 7(3); 241-250.

40. Flynn KC et al. “ADF/Cofilin-Mediated Actin Retrograde Flow Directs Neurite Formation in the Developing Brain.” *Neuron*. 2012, 76(6); 1091-1107.

41. Garvalov BK, Flynn KC, Neukirchen D, Meyn L, Teusch N, Wu X, Brakebusch C, Bamburg JR, Bradke F. “Cdc42 regulates cofilin during the establishment of neuronal polarity.” *J Neuroscience*. 2007, 27(48); 13117-13129.

42. Bravo-Cordero JJ, Magalhaes MAO, Eddy RJ, Hodgson L, Condeelis J. “Functions of cofilin in cell locomotion and invasion.” *Nat Rev Mol Cell Biol*. 2013, 14(7); 405-415.

43. Flynn KC. “The cytoskeleton and neurite initiation.” *BioArchitecture*. 2013, 3(4); 86-109.

44. Gomez TM and Letourneau PC. “Actin Dynamics in Growth Cone Motility and Navigation.” *J Neurochem*. 2014, 129(2); 221-234.

45. Bosch M, Castro J, Saneyoshi T, Matsuno H, Sur M, Hayashi Y. “Structural and Molecular Remodeling of Dendritic Spine Substructures during Long-Term Potentiation.” *Neuron*. 2014, 82; 444-459.

46. Calabrese B, Saffin JM, Halpain S. “Activity-Dependent Dendritic Spine Shrinkage and Growth Involve Downregulation of Cofilin via Distinct Mechanisms.” *PLoS One*. 2014, 9(4); e94787.

47. Lamprecht Raphael. “The actin cytoskeleton in memory formation.” *Progress in Neurobiology*. 2014, 117; 1-19.

48. Bamburg JR and Bloom GS. “Cytoskeletal pathologies of Alzheimer disease.” *Cell Motil Cytoskel.* 2009, 66; 635-649.

49. Minamide LS, Maiti S, Boyle JA, Davis RC, Coppinger JA, Bao Y, Huang TY, Yates J, Bokoch GM, Bamburg JR. “Isolation and Characterization of Cytoplasmic Cofilin-Actin Rods.” *Journal of Bio Chem*. 2010, 285(8); 5450-5460.

50. Bernstein BW, Shaw AE, Minamide LS, Pak CW, Bamburg JR. “Incorporation of Cofilin into Rods Depends on Disulfide Intermolecular Bonds: Implications for Actin Regulation and Neurodegenerative Disease.” *J. Neuroscience*. 2012, 32(19); 6670-6681.

51. Minamide LS, Striegl AM, Boyle JA, Meberg PJ, Bamburg JR. “Neurodegenerative stimuli induce persistent ADF/cofilin-actin rods that disrupt distal neurite function.” Nat *Cell Bio*. 2000, 2; 628-636.

52. Davis et al. “Amyloid Beta dimers/trimers potently induce cofilin-actin rods that are inhibited by maintaining cofilin phosphorylation.” *Molecular Neurodegeneration*. 2011, 6; 10.

53. Maloney MT, Minamide LS, Kinley AW, Boyle JA, Bamburg JR. “Beta-secretase-Cleaved AMyloid Precursor Protein Accumulates at Actin Inclusions Induced in Neurons by Stress or Amyloid Beta: A Feedforward Mechanism for Alzheimer’s Disease.” *J. Neuroscience*. 2005, 25(49); 11313-11321.

54. Walsh KP, Minamide LS, Kane SJ, Shaw AE, Brown DR, Pulford B, Zabel MD, Lambeth JD, Kuhn TB, Bamburg JR. “Amyloid-beta and Proinflammatory Cytokines Utilize a Prion Protein-Dependent Pathway to Activate NADPH Oxidase and Induce Cofilin-Actin Rods in Hippocampal Neurons.” *PLoS One*. 9(4); e95995.

55. Bernstein BW and Bamburg JR. “ADF/Cofilin: A Functional Node in Cell Biology.” *Trends in Cell Biol*. 2010, 20(4); 187-195.

56. Jang D, Han J, Lee S, Lee Y, Park H, Lee S, Kim H, Kaang B. “Cofilin expression induces cofilin-actin rod formation and disrupts synaptic structure and function in Aplysia synapses.” *PNAS*. 2005, 102(44); 16072-16077.

57. Fulga et al. “Abnormal bundling and accumulation of F-actin mediates tau-induced neuronal degeneration in vivo.” *Nature Cell Biology*. 2007, 9(2); 139-148.

58. Davis et al. “Mapping Cofilin-Actin Rods in Stressed Hippocampal Slices and the Role of cdc42 in Amyloid-beta-Induced Rods.” *J Alzheimers Dis*. 2009, 18(1); 35-50.

59. Andersen JK. “Oxidative stress in neurodegeneration: cause or consequence?” *Nature Rev Neuroscience*. 2004, 5; S18-S25.

60. Keller JN, Schmitt FA, Scheff SW, Ding Q, Chen Q, Butterfield DA, Markesbery WR. “Evidence of increased oxidative damage in subjects with mild cognitive impairment.” *Neurology*. 2005, 64; 115-1156.

61. Ansari MA and Scheff SW. “Oxidative Stress in the Progression of Alzheimer Disease in the Frontal Cortex.” *J Neuropathol Exp Neurol*. 2010, 69(2); 155-167.

62. Block ML. “NADPH oxidase as a therapeutic target in Alzheimer’s disease.” *BMB Neuroscience*. 2008, 9 (Supp 2); S8.

63. Hensley K, Carney JM, Mattson MP, Aksenova M, Harris M, Wu JF, Floyd RA, Butterfield DA. “A model for beta-amyloid aggregation and neurotoxicity based on free radical generation by the peptide: Relevance to Alzheimer disease.” *Proc Natl Acad Sci*. 1994, 91; 3270-3274.

64. Shimohama S et al. “Activation of NADPH Oxidase in Alzheimer’s Disease Brains.” *Biochemical and Biophysical Research Communications*. 2000, 273; 5-9.

65. Cheng X, Shen Y, Li R. “Targeting TNF: a Therapeutic strategy for Alzheimer’s disease.” Drug Discovery Today. 2014, 1-6.

66. Ansari MA, Scheff SW. “NADPH oxidase activation and cognition in Alzheimer disease progression.” *Free Radic Biol Med.* 2011, 51; 171-178.

67. Angeloni C, Prata C, Sega FVD, Pepermo R, Hrelia S. “Traumatic Brain Injury and NADPH Oxidase: A Deep Relationship.” *Oxid Med Cell Longev*. 2015, 370312.

68. Ansari MA, Roberts KN, Scheff SW. (2014) “A time course of NADPH-oxidase up-regulation and endothelial nitric oxide synthase activation in the hippocampus following neurotrauma.” *Free Radic Biol Med*. 2014, 77; 21-9.

69. Zhao L, Ma QL, Calon F, Harris-White ME, Yang F, Lim GP, Morihara T, Ubeda OJ, Ambeqaokar S, Hansen JE, Weisbart RH, Teter B, Frautschy SA, Cole GM. “Role of p21-activated kinase pathway defects in the cognitive deficits of Alzheimer disease.” *Nature Neuroscience*. 2006, 9(2); 234-242.

70. Huang TY, Minamide LS, Bamburg JR, Bokoch GM. “Chronophin mediates an ATP-sensing mechanism for cofilin dephosphorylation and neuronal cofilin-actin rod formation.” *Dev Cell*. 2008, 15(5); 691-703.

71. Kim JS, Huang TY, Bokoch GM. “Reactive oxygen species regulate a slingshot-cofilin activation pathway.” *Mol Bio Cell*. 2009, 20(11); 2650-2660.

72. Yao J, Hennessey T, Flynt A, Lai E, Beal MF, Lin MT. “MicroRNA-related cofilin abnormality in Alzheimer’s disease.” *PLos One*. 2010, 5(12); e15546.

73. Panday A, Sahoo MK, Osorio D, Batra S. “NADPH oxidases: an overview from structure to innate immunity-associated pathologies.” *Cellular & Molecular Immunology*. 2015, 12: 5-23.

74. Cahill-Smith S and Li JM. “Oxidative stress, redox signalling and endothelial dysfunction in ageing-related neurodegenerative diseases: a role of NADPH oxidase 2.” *BJCP*. 2014, 78 (3); 441-453.

75. Sumimoto H. “Structure, regulation and evolution of Nox-family NADPH oxidases that produce reactive oxygen species.” *FEBS J*. 2008, 275; 3249-3277.

76. Sumimoto H, Miyano K, Takeya R. “Molecular composition and regulation of the Nox family NAD(P)H oxidases.” *Biochemical and Biophysical Research Communications*. 2005, 338; 677-686.

77. Morgan MH, Kim YS, Liu Z. “TNF-α and reactive oxygen species in necrotic cell death.” *Cell Research*. 2008, 18; 343-349.

78. Shaw AE, Minamide LS, Bill CL, Funk JD, Maiti S, Bamburg JR. “Cross-reactivity of antibodies to actin-depolymerizing factor/cofilin family proteins and identification of the major epitope recognized by a mammalian actin-depolymerizing factor/cofilin antibody.” *Electrophoresis*. 2004, 25(15); 2611-2620.

79. McKhann G, Drachman D, Folstein M, et al. “Clinical diagnosis of Alzheimer's disease: report of the NINCDS-ADRDA Work Group under the auspices of Department of Health and Human Services Task Force on Alzheimer's Disease.” *Neurology*. 1984, 34; 939–944.

80. Minamide LS et al. “Production and use of replication-deficient adenovirus for transgene expression in neurons.” *Methods Cell Biology*. 2003, 71; 387-416.

81. Rahman et al. “Cofilin Rods and Aggregates Concur with Tau Pathology and the Development of Alzheimer’s Disease.” *J of Alzheimer’s Disease*. 2014, 42; 1443-1460.

82. Li et al. “Post-mortem Interval Effects on the Phosphorylation of Signaling Proteins.” *Neuropsychopharmacology*. 2003, 28; 1017-1025.

83. Corina et al. “Effects of Postmortem Interval on Biomolecule Integrity in the Brain.” *Journal of Neuropathology & Experimental Neurology*. 2015, 74(5); 459-469.

84. Braak H and Braak E. “Neuropathological stageing of Alzheimers-related changes.” *Acta Neuropathol*. 1991, 82; 239-259.

85. Ridderinkhof KR, Wildenberg WPM, Segalowitz SJ, Carter CS. “Neurocognitive mechanisms of cognitive control: The role of prefrontal cortex in action selection, response inhibition, performance monitoring and reward-based learning.” *Brain and Cognition*. 2004, 56(2); 129-140.

86. Etkin A, Egner T, Kalisch R. “Emotional processing in anterior cingulate and medial prefrontal cortex.” *Cell*. 2011, 15(2); 85-93.

87. Buckner RL, Kelley WM, Petersen SE. “Frontal cortex contributes to human memory formation.” *Nature Neuroscience*. 1999, 2(4); 311-314.

88. Schmitt FA et al. “‘Preclinical’ AD revisited: Neuropathology of cognitively normal older adults.” *Neurology*. 2000, 55(3); 370-376.

89. Litersky JM, Johnson GVW, Jakes R, Goedert M, Lee M, Seubert P. “Tau protein is phosphorylated by cyclin AMP-dependent protein kinase calcium/calmodulin-dependent protein kinase II within its microtubule binding domains at Ser-262 and Ser-356.” *Biochem J*. 1996, 318; 655-660.

90. Abe, H and Obinata, T. “An actin-depolymerizing protein in embryonic chicken skeletal muscle: purification and characterization.” *J Biochem*. 1989, 106; 172-180.

91. Vogt BA, Nimchinsky EA, Vogt LJ, Hof PR. “Human Cingulate Cortex: Surface Features, Flat Maps, and Cytoarchitecture.” *The Journal of Comparative Neurology*. 1995, 359; 490-506.

92. Chana G, Landau S, Beasley C, Everall IP, Cotter D. “Two-Dimensional Assessment of Cytoarchitecture in the Anterior Cingulate Cortex in Major Depressive Disorder, Bipolar Disorder, and Schizophrenia: Evidence for Decreased Neuronal Somal Size and Increased Neuronal Density.” *Society of Biological Psychiatry*. 2003, 53; 1086-1098.

93. Pal R, Thakur PB, Li S, Minard C, Rodney GG. “Real-Time Imaging of NADPH Oxidase Activity in Living Cells Using a Novel Fluorescent Protein Reporter.” *PLoS ONE*. 2013, 8:e63989.

94. Chung K et al. “Structural and molecular interrogation of intact biological systems.” *Nature*. 2013, 497(7449); 332-337.